

REPORT DOCUMENTATION PAGE		READ INSTRUCTIONS BEFORE COMPLETING FORM
1. REPORT NUMBER TR 7217	2. GOVT ACCESSION NO.	3. RECIPIENT'S CATALOG NUMBER
4. TITLE (and Subtitle) ANALYSIS AND SIMULATION OF TIME DELAY ESTIMATION WITH COMPENSATION FOR SOURCE/RECEIVER RELATIVE MOTION		5. TYPE OF REPORT & PERIOD COVERED
		6. PERFORMING ORG. REPORT NUMBER
7. AUTHOR(s) Roger J. Tremblay		8. CONTRACT OR GRANT NUMBER(s)
9. PERFORMING ORGANIZATION NAME AND ADDRESS Naval Underwater Systems Center New London Laboratory New London, Connecticut 06320		10. PROGRAM ELEMENT, PROJECT, TASK AREA & WORK UNIT NUMBERS
11. CONTROLLING OFFICE NAME AND ADDRESS		12. REPORT DATE 24 July 1984
		13. NUMBER OF PAGES
14. MONITORING AGENCY NAME & ADDRESS (if different from Controlling Office)		15. SECURITY CLASS. (of this report) UNCLASSIFIED
		15a. DECLASSIFICATION/DOWNGRADING SCHEDULE
16. DISTRIBUTION STATEMENT (of this Report) Approved for public release; distribution unlimited.		
17. DISTRIBUTION STATEMENT (of the abstract entered in Block 20, if different from Report)		
18. SUPPLEMENTARY NOTES		
19. KEY WORDS (Continue on reverse side if necessary and identify by block number) Source/Receiver Relative Motion Time Delay Estimation		
20. ABSTRACT (Continue on reverse side if necessary and identify by block number) Time Delay Estimation (TDE) has received considerable attention in recent years, primarily because of its applicability to source position estimation in passive sonar. This paper presents the more significant related theory and analysis developed recently in this area. The two broad classes of (1) TDE when the source and receivers are in relatively fixed positions and (2) TDE when there is relative motion between the source and receivers are considered, with emphasis on the latter, more general class.		

NUSC Technical Report 7217
24 July 1984

LIBRARY
RESEARCH REPORTS DIVISION
NAVAL POSTGRADUATE SCHOOL
MONTEREY, CALIFORNIA 93943

Analysis and Simulation of Time Delay Estimation With Compensation for Source/Receiver Relative Motion

Roger J. Tremblay
Surface Ship Sonar Department



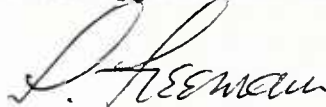
Naval Underwater Systems Center
Newport, Rhode Island / New London, Connecticut

Preface

This study was prepared as a dissertation in partial fulfillment of the requirements for the degree Master of Science in Electrical Engineering at the University of Washington. The work presented here was funded by the Naval Underwater Systems Center as part of the Long Term Training program.

The author acknowledges the contributions of those individuals who supported the completion of this research: Professor Dean W. Lytle for his guidance in the preparation of this report; Dr. Kent Scarbrough, Dr. John Betz, and Mr. Steve Robison for their valuable technical contributions; Mr. Jay Melillo for his assistance; and Dr. G. Clifford Carter for his administrative support, technical guidance, and encouragement.

Reviewed and Approved: 24 July 1984

A handwritten signature in dark ink, appearing to read "L. Freeman", is written over the printed name.

L. Freeman
Head, Surface Ship Sonar Department

The author of this report is located at the
New London Laboratory, Naval Underwater Systems Center,
New London, Connecticut 06320.

TABLE OF CONTENTS

	<u>Page</u>
List of Figures	iv
List of Tables.	v
List of Acronyms.	vi
Introduction.	1
1.0 APPLICATION OF TIME DELAY ESTIMATION TO SONAR.	2
2.0 TIME DELAY ESTIMATION WITH FIXED SOURCE AND RECEIVERS	10
2.1 Some Frequency Weightings Used in Cross-Correlations	11
2.2 Derivation of Generalized Cross- Correlation (GCC) as a Maximum Likelihood Estimate	17
2.3 Performance of the GCC Time Delay Estimator.	28
3.0 TIME DELAY ESTIMATION WITH MOVING SOURCE AND/OR RECEIVERS.	39
3.1 Motion Model.	39
3.2 Compensating for Relative Time Companding	43
3.3 Compensating for Varying Time Delay.	46
3.3.1 Compensation in the Frequency Domain (Phase Rotation).	53
3.3.2 Compensation in the Delay Domain (Deskewing).	54

TABLE OF CONTENTS (continued)

	<u>Page</u>
4.0 SIMULATION OF MOTION COMPENSATED TIME DELAY ESTIMATION	58
4.1 Simulation Description.	58
4.1.1 Signal Generation	58
4.1.2 Processing.	59
4.1.3 Simulation Run Parameters	60
4.1.4 Results	60
4.1.5 Discussion.	64
5.0 CONCLUSIONS AND RECOMMENDATIONS.	67
LIST OF REFERENCES	69
APPENDIX A: Simulation Program Description	73

LIST OF FIGURES

	<u>Page</u>
1. Planar Model.	4
2. Multiple Source Positions with Same Delay . .	6
3. Source/Receiver Geometry.	7
4. Bearing Angle for Large Range	8
5. Generalized Cross-Correlator Block Diagram. .	12
6. Anomalous Peaks in the Cross-Correlation Function.	30
7. CPE vs. CRLB.	33
8. CPE and CRLB for Various Integration Times. .	35
9. CPE and CRLB vs. Simulation Results	36
10. Coherent and Incoherent Integration Performance	37
11. Time-Companding Compensation Block Diagram. .	45
12. Step-wise Constant Approximation of Delay Rate.	49
13. Example Short-time Cross-Correlation Functions	51
14. Uncompensated Short-time Cross-Correlation Functions (Averaged).	52
15. Phase Rotation Compensation Block Diagram . .	55
16. Deskewing Compensation Block Diagram.	57
17. Compensated Short-Time Cross- Correlations (Phase Rotation Method).	61
18. Sample Ambiguity Surface.	62
19. Compensated vs. Uncompensated Performance, Simulation Results.	65
A.1 Program Structure Chart	74
A.2 Functional Flow Chart	75

LIST OF TABLES

<u>Number</u>		<u>Page</u>
1.	Some Frequency Weighting Functions for Cross-Correlation	13
2.	Simulation Run Statistics	63

LIST OF ACRONYMS

ASSP	Acoustics Speech and Signal Processing
COV	Covariance matrix
CPE	Correlation Performance Estimate
CRLB	Cramér-Rao Lower Bound
dB	Decibels
DSTC	Deskewed Short Time Correlator
FFT	Fast Fourier Transform
GCC	Generalized Cross-Correlation
HT	Hannan-Thomson
Hz	Hertz
ML	Maximum Likelihood
pdf	Probability density function
PHAT	Phase Transform
RTC	Relative Time Companding
SCC	Standard Cross-Correlation
SCOT	Smoothed Coherence Transform
SNR	Signal-to-Noise Ratio
Stdv[]	Standard Deviation of []
TDE	Time Delay Estimation
TDOA	Time Difference of Arrival
Var[]	Variance of []

INTRODUCTION

Time Delay Estimation (TDE) has received considerable attention in recent years, primarily because of its applicability to source position estimation in passive sonar. This paper presents the more significant related theory and analysis developed recently in this area. The two broad classes of (1) TDE when the source and receivers are in relatively fixed positions and (2) TDE when there is relative motion between the source and receivers are considered, with emphasis on the latter, more general class. By way of background, a brief description of the typical sonar problem which has motivated much of the research in this area is given. Next the no motion case is studied, followed by analysis for the case with motion. Finally, a computer implementation of a motion compensated cross-correlator is presented and results which corroborate the theory and analysis are presented and discussed. A brief computer program description is provided in Appendix A.

1.0 APPLICATION OF TIME DELAY ESTIMATION TO SONAR

Sonar systems may be divided into two major categories: Active Sonar and Passive Sonar. In Active Sonar, a pre-determined signal is transmitted by the sonar into the ocean environment. The received echo from objects in the ocean is then analyzed to obtain information about the objects such as their nature, location, and movement. Since the form of the signal can be controlled, it can be designed to best meet some desired performance criteria such as detectability and spatial resolution. The distance to an object is determined by measuring the total travel time of the signal, from the transmitter to the object and back to the sonar receiver, and utilizing knowledge of the speed of sound in water. The angle to the object can be determined by processing the received data only in certain angular directions (a process referred to as beamforming). The major drawback of Active Sonar is that the location of the sonar is given away when it transmits, a very undesirable effect for military applications. Also, its performance can be greatly limited by reverberation of the transmitted signal, especially for high-powered transmitters in shallow water or in an area with many scatterers, such as particulate matter and biologics.

The alternative to Active Sonar is Passive Sonar which "listens" for sounds emanating from the objects themselves, such as flow noise, machinery noise, and marine life noises. The signal is typically processed by spectral analysis to determine the characteristics of the objects. A major limitation to Passive Sonar is a lack of complete knowledge of the characteristics of the signal, requiring more flexibility in the processing. Additionally, since the travel

time of the received signal is not known, the distance to the source cannot be measured directly. Instead, multiple, accurate bearings to the source must be measured, from which a range can be determined indirectly. It is primarily for the purpose of obtaining these accurate bearings that Time Delay Estimation (TDE) is employed in Passive Sonar. References [1], [2], [3], and [4] contain extensive material on sonar and related signal processing. Reference [5] contains many papers on TDE and provides an excellent overview of much of the more recent work on the subject; in particular, the article by Carter summarizes TDE as applied to Passive Sonar.

Figure 1 illustrates the basic model used for analysis of passive TDE. The source and two receivers, with a single propagation path to each receiver, are all assumed to lie in the same plane. In this planar model it is also assumed that there is no relative motion among the source and receivers. The signal, $s(t)$, arrives at Receiver 1 then at Receiver 2 at a time D later. For a distant source the attenuation, α , of the signal arriving at Receiver 2 is $\cong 1$. Also input at each receiver are noise $n_1(t)$ and $n_2(t)$, which are assumed to be uncorrelated with each other and the signal. The signal and noise are also assumed to be zero-mean, wide-sense stationary, broadband random processes. The equations for the model are

$$r_1(t) = s(t) + n_1(t) \quad (1.1.a)$$

$$r_2(t) = s(t + D) + n_2(t) \quad (1.1.b)$$

There are more than one possible source locations for which the same time delay value, D , would occur between

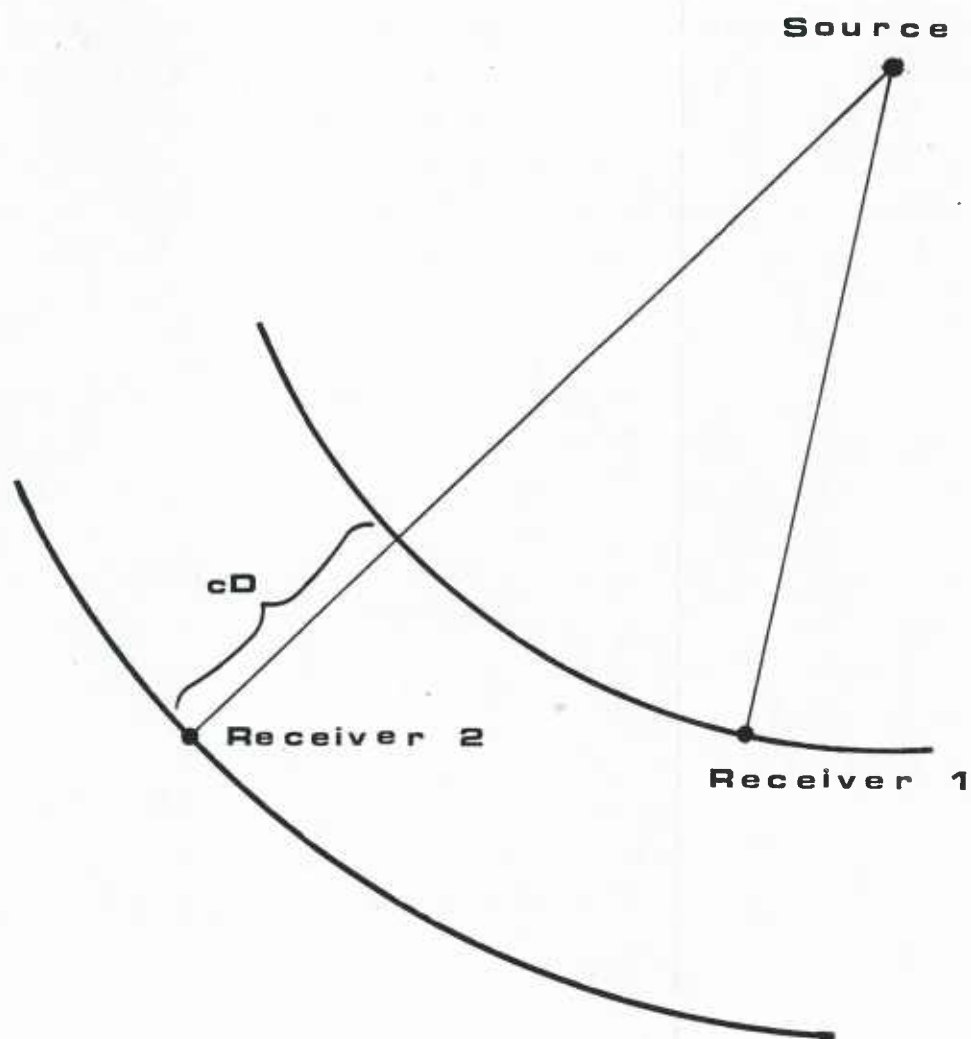


FIGURE 1
PLANAR MODEL

arrivals at the two receivers [6], as illustrated in Figure 2. In fact, the source could be anywhere on the locus of points that form a hyperbola. Figure 3 shows the geometry from which the equation for the hyperbola and the equation for the bearing to the source (measured from the midpoint between the receivers) for any point on the hyperbola can be derived. The difference in the range between the source and Receiver 1 and Receiver 2 is

$$R_2 - R_1 = cD$$

where c is the speed of sound in water, D is the time delay.

Substituting for R_2 and R_1 , the equivalent Euclidian distance for the given coordinates

$$\begin{aligned} \sqrt{(X+L/2)^2 + Y^2} - \sqrt{(X-L/2)^2 + Y^2} &= cD \\ (4/c^2 D^2) X^2 - [4/(4(L/2)^2 - c^2 D^2)] Y^2 &= 1. \end{aligned} \quad (1.2)$$

Equation (1.2) defines a hyperbola. The bearing angle θ is found from

$$\cos(\theta) = (cD/L) [1 + (L/2R)^2 - (cD/2R)^2]^{1/2}$$

As seen in Figure 4, if the distance to the source is large compared to the receiver separation (i.e., $R \gg L$, as is usually the case), then the bearing is approximated by the angles formed by two straight lines which form asymptotes to the hyperbola. This bearing then is related to the time delay D , and the sensor separation, L , by

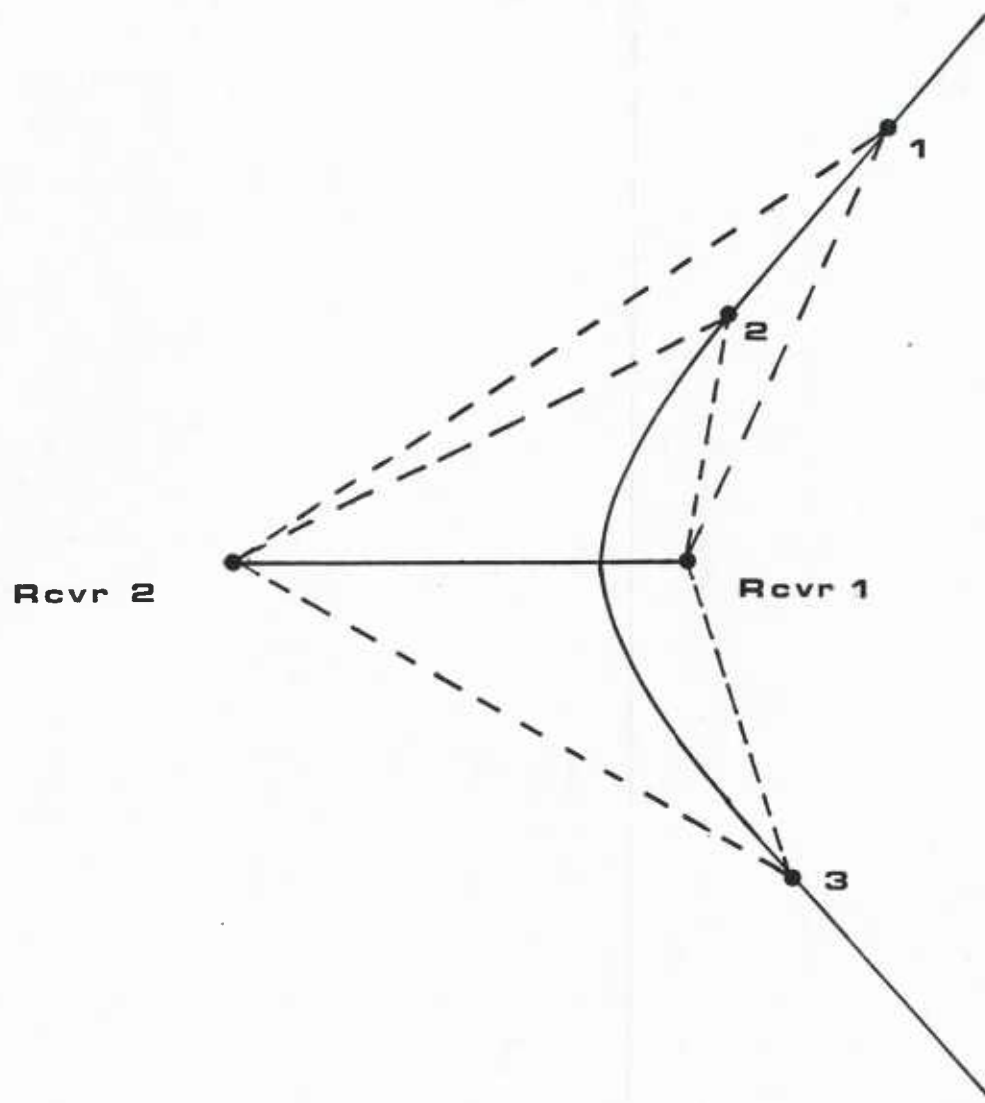


FIGURE 2
MULTIPLE SOURCE POSITIONS WITH SAME DELAY

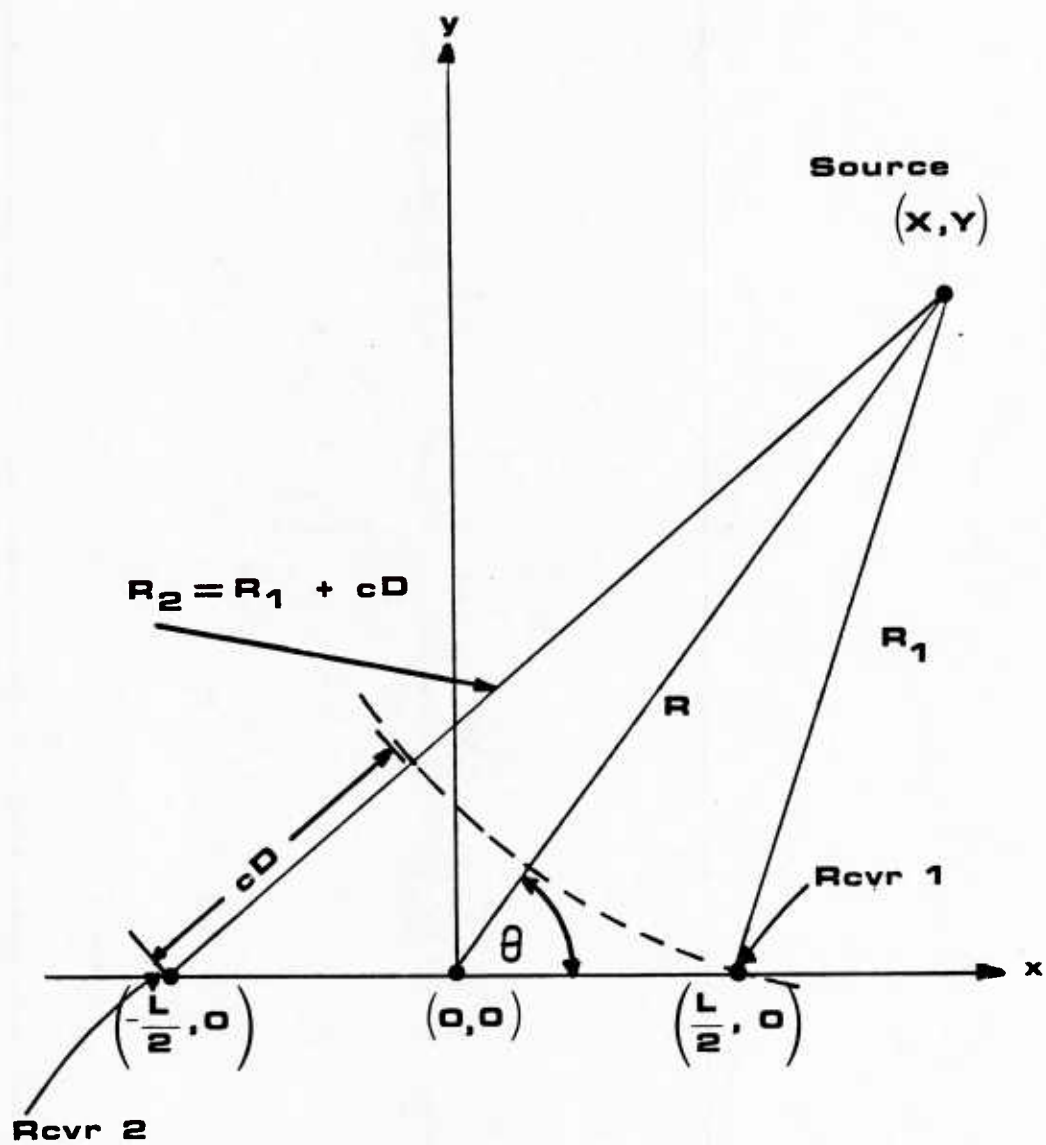


FIGURE 3
SOURCE/RECEIVER GEOMETRY

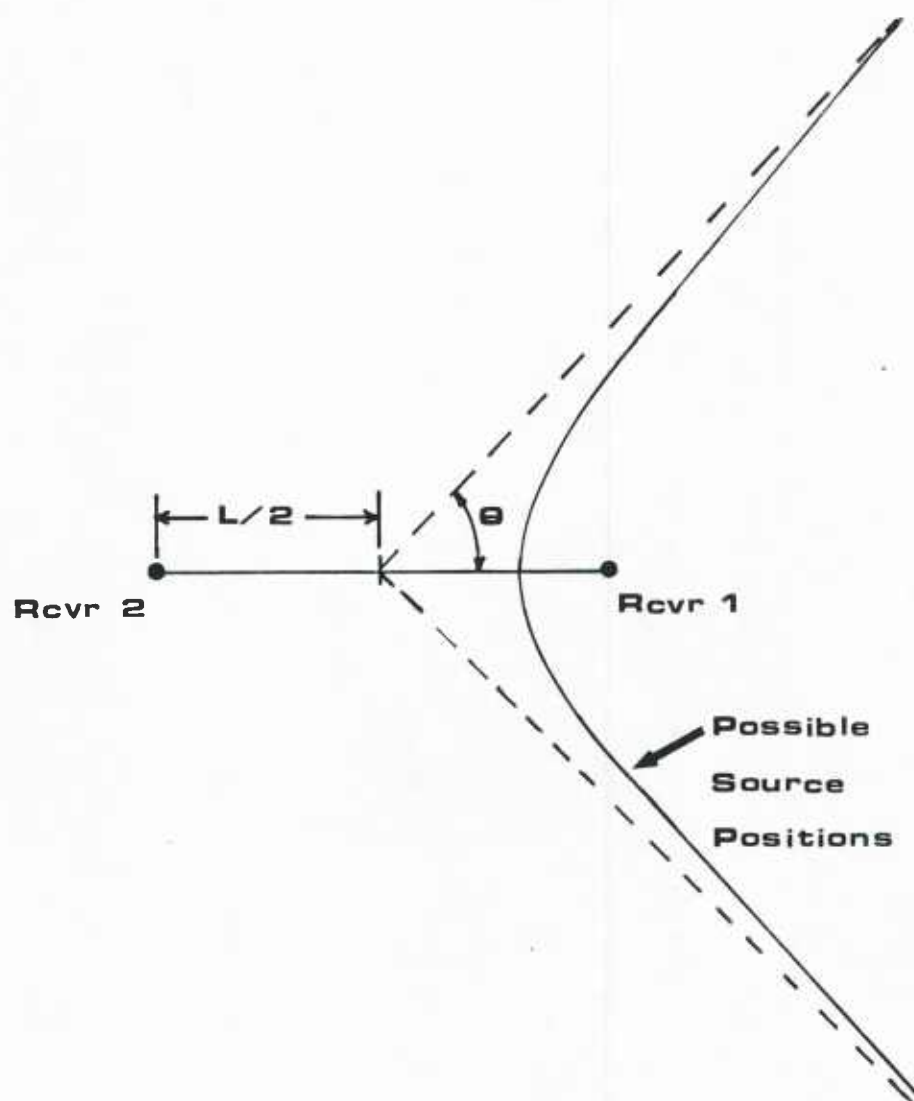


FIGURE 4
BEARING ANGLE FOR LARGE RANGE

$$\cos(\theta) \cong (cD/L)$$

$$\theta \cong \cos^{-1} (cD/L) \quad (1.3)$$

where c is the speed of sound in the ocean. Thus, for known sensor spacing, L , an estimate of the time delay yields the bearing to the source (albeit, it is an ambiguous bearing which must be resolved by other means such as ship maneuvers, or auxiliary information like rough bearings from passive beamforming). If three co-linear receivers are used, then ranging is possible by using two bearings and the sensor spacing for a triangulation [5, pp. 463-470].

2.0 TIME DELAY ESTIMATION WITH FIXED SOURCE AND RECEIVERS

The most common method for estimating time delay passively is to compute the cross-correlation of the signal from two spatially separated receivers. A generalized method for estimating time-delay with cross-correlation was described by Knapp and Carter [7], and is recounted here.

For the model defined by (1.1)

$$R_{r_1 r_2}(t_1, t_2) = E [r_1(t_1) r_2(t_2)]$$

The value of $\tau = t_1 - t_2$ which gives the maximum value for the cross-correlation is chosen as the estimate of the true delay, D .

Since we are always limited to a finite observation time, $R_{r_1 r_2}(\tau)$ must be estimated. For ergodic processes, this is computed by:

$$\hat{R}_{r_1 r_2}(\tau) = \frac{1}{T-\tau} \int_{\tau}^T r_1(t) r_2(t-\tau) dt \quad (2.1)$$

where T is the finite observation time. This estimation of $\hat{R}_{r_1 r_2}(\tau)$ plus the presence of noise will result in errors in the computation of \hat{D} , the delay estimate. In practice, $\hat{R}_{r_1 r_2}(\tau)$ is computed from the inverse Fourier transform of the estimate of the cross-spectrum, $\hat{G}_{r_1 r_2}(f)$, by:

$$\hat{R}_{r_1 r_2}(\tau) = \int_{-\infty}^{\infty} \hat{G}_{r_1 r_2}(f) e^{j2\pi f\tau} df \quad (2.2)$$

In order to reduce the error in $\hat{R}_{r_1 r_2}(\tau)$, and thus improve the accuracy of \hat{D} , we can pre-filter $r_1(t)$ and $r_2(t)$ prior

to cross-correlating. The pre-filters would be selected to emphasize frequencies where the signal-to-noise-ratio (SNR) is highest and de-emphaize them where it is low. Figure 5 illustrates such a configuration.

For pre-filters $H_1(f)$ and $H_2(f)$, which operate on $r_1(t)$ and $r_2(t)$ and give outputs $y_1(t)$ and $y_2(t)$, respectively, the cross-spectrum is then

$$G_{y_1 y_2}(f) = H_1(f) H_2^*(f) G_{r_1 r_2}(f) \quad (2.3)$$

and the cross-correlation is computed from

$$\hat{R}_{y_1 y_2}(\tau) = \int_{-\infty}^{\infty} W(f) \hat{G}_{r_1 r_2}(f) e^{j2\pi f\tau} df \quad (2.4)$$

where $W(f) = H_1(f) H_2^*(f)$. Thus, the prefiltering can be done as frequency weighting in the frequency domain. Equation (2.4) is referred to as the Generalized Cross-Correlation (GCC) function, and $W(f)$, the General Frequency Weighting, which is chosen to optimize some performance criterion.

2.1 Some Frequency Weightings Used In Cross-Correlation

Table 1 lists several proposed frequency weightings. Each is described in detail in [7]. As the weightings are functions of the signal and noise spectra, it must be kept in mind that, in practice, the weightings themselves must be estimated (unless there is sufficient prior knowledge of the spectra). The major features of each are outlined in the following.

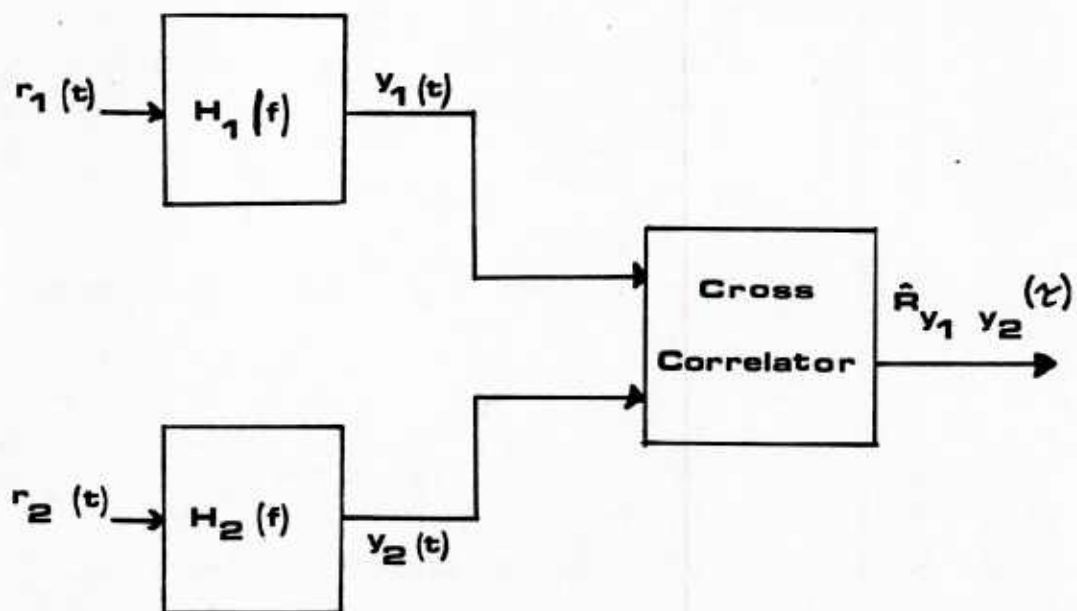


FIGURE 5
GENERALIZED CROSS-CORRELATION FUNCTION

PROCESSOR	WEIGHT: $W(f) = H_1(f)H_2^*(f)$
CROSS-CORRELATION	1
ROTH	$\frac{1}{G_{r1r1}(f)}$
SCOT	$\frac{1}{\sqrt{G_{r1r1}(f) G_{r2r2}(f)}}$
PHAT	$\frac{1}{ G_{r1r2}(f) }$
ECKART	$\frac{G_{ss}(f)}{[G_{n1n1}(f)G_{n2n2}(f)]}$
ML or HT	$\frac{C_{r1r2}(f)}{ G_{r1r2}(f) [1-C_{r1r2}(f)]}$

TABLE 1
SOME FREQUENCY WEIGHTING FUNCTIONS FOR CROSS-CORRELATION

The first weighting, $W(f) = 1$ is, of course, no weighting at all and is used when the signal and noise have flat spectra, equal bandwidths and the SNR is constant across the entire band. It is often referred to as the Standard Cross-Correlation (SCC).

The Roth processor [8], which gives correlation estimate

$$\hat{R}_{y_1 y_2}(\tau) = \int_{-\infty}^{\infty} \frac{\hat{G}_{r_1 r_2}(f)}{G_{r_1 r_1}(f)} e^{2\pi f \tau} df$$

is also the estimate of the impulse response of the filter

$$H(f) = \frac{G_{r_1 r_2}(f)}{G_{r_1 r_1}(f)}$$

which is an optimum approximation of the linear mapping of $r_1(t)$ to $r_2(t)$ (Wiener-Hopf filter). Since

$$G_{r_1 r_1}(f) = G_{ss}(f) + G_{n_1 n_1}(f)$$

we get

$$\hat{R}_{y_1 y_2}(\tau) = \int_{-\infty}^{\infty} \frac{\hat{G}_{r_1 r_2}(f)}{G_{ss}(f) + G_{n_1 n_1}(f)} e^{2\pi f \tau} df$$

This weighting can be seen to suppress those frequencies where the noise at receiver 1 is highest.

The Smooth Coherence Transform (SCOT) [9], [10] processor can be seen to suppress frequencies where the noise in either or both channels is high. The process is equivalent to "pre-whitening" the inputs $r_1(t)$ and $r_2(t)$ by

$$H_1(f) = 1/G_{r_1r_1}(f) \text{ and } H_2(f) = 1/G_{r_2r_2}(f)$$

and then cross-correlating the results. For the case of white signal plus non-white noise, the effect of pre-whitening is to attenuate the cross-spectrum estimate where the noise is highest and conversely where it is lowest. If $G_{r_1r_1}(f) = G_{r_2r_2}(f)$, the SCOT can be seen to be equivalent to the Roth processor.

The Phase Transform (PHAT) [10] window was developed specifically to minimize the spreading of the correlation peak caused by non-white signal. For the ideal case of white signal and no noise, the cross-correlation is a delta function, $\delta(\tau - D)$. A non-white signal results in the spreading or smearing of the delta function through convolution with the transform of the signal spectrum. For perfect estimation, where $\hat{G}_{r_1r_2}(f) = G_{r_1r_2}(f)$, then

$$\frac{\hat{G}_{r_1r_2}(f)}{|G_{r_1r_2}(f)|} = e^{j2\pi fD} = e^{j\theta(f)}.$$

That is we get unit magnitude with linear phase. Then $R_{y_1y_2}(\tau) = \delta(\tau - D)$ and no spreading takes place. In practice, though, $\hat{G}_{r_1r_2}(f) \neq G_{r_1r_2}(f)$, and $\theta(f) \neq 2\pi fD$, but is erratic, resulting in a correlation which is not a delta function. Another serious problem with the PHAT is that it

weights $\hat{G}_{r1r2}(f)$ as the inverse of $G_{ss}(f)$, thus accentuating, rather than attenuating the frequency regions where the signal is weakest.

The weighting referred to as the Eckart Filter [11] has the characteristic of maximizing the ratio of the change in the mean of the correlator output when signal is present, to the standard deviation of the correlator output when there's noise alone. Like the SCOT, this processor suppresses frequencies where the noise is highest, but, additionally, it gives zero weighting to the regions where $G_{ss}(f) = 0$.

The last weighting function, the HT (for the originators Hannan and Thompson [12]) is shown in the next section to be a maximum likelihood estimator of the delay, D , when the assumption of Gaussian noise and signal is made. It is also shown that the variance of the delay estimate, $\text{Var}[\hat{D}]$ is equal to the Cramér-Rao Lower Bound (CRLB), and, as such, it is an optimum (minimum variance) estimator (see next section). It's use of the magnitude squared coherence,

$$C_{r1r2}(f) = \frac{|G_{r1r2}(f)|^2}{G_{r1r1}(f) G_{r2r2}(f)} \quad (2.5)$$

between the receivers serves to emphasize the high SNR regions while attenuating the low, like the SCOT. Like the PHAT, the $|G_{r1r2}(f)|$ term in the denominator tends to reduce the spreading of the correlation peak, but in this case, it suppresses the regions where the phase, $\theta(f)$, is most erratic, (namely the low or zero SNR regions) by the coherence terms.

For the case where the SNR is low and $\alpha = 1$, the HT and Eckart processors can be shown to be equivalent [7]. Additionally, at low SNR, they could be interpreted as SCOT processors with added SNR weighting or as PHAT processors with added SNR^2 weighting. These processors have recently been implemented and analyzed as described in [13], [14], [15] and [16].

2.2 Derivation of Generalized Cross-Correlation (GCC) as a Maximum Likelihood Estimate

Knapp and Carter [7] derive the Maximum Likelihood (ML) estimate for time delay, which proves to be the same as that proposed by Hannan and Thompson. This derivation is summarized by Scarbrough [13] with some added clarification and is presented here in a slightly modified form.

Outlining briefly, the assumption that the signal and noise are Gaussian processes is made in addition to the previous assumption of being wideband, wide sense stationary, zero-mean, and uncorrelated with each other. We will determine an observation vector, \underline{R} , which depends upon the true time delay, D , and the signal and noise auto- and cross-power spectra, which are assumed known. A maximum likelihood (ML) estimate of the delay is made by picking as our estimate the hypothesized delay, τ , which maximizes the probability density function (pdf) of \underline{R} conditioned on τ . It will be seen that the estimator reduces to picking the τ which maximizes the cross-correlation function of the receiver signals whose cross-spectrum has been multiplied by a weighting function formed from the auto- and cross-spectra of the signal and noise. Furthermore, it will be seen that the variance of this ML estimate of delay achieves the

Cramér-Rao Lower Bound (CRLB) and, as such, is the optimum estimator, in a minimum variance sense.

Our first step is to express the received waveforms, $r_1(t)$ and $r_2(t)$ over the interval, $0 \leq t \leq T$, by their Fourier Series coefficients. This can be done by forming the periodic extension:

$$\tilde{r}_i(t+mT) = R_i(t), \quad 0 \leq t \leq T, \quad i = 1, 2$$

for any integer value of m . The Fourier Series coefficients for these periodic extensions are then

$$R_i(k) = 1/T \int_0^T \tilde{r}_i(t) e^{-jk2\pi f_0 t} dt, \quad i = 1, 2 \quad (2.6)$$

where

$$f_0 = 1/T$$

The two received signals $r_i(t)$, $i = 1, 2$ can be computed from these Fourier coefficients by taking one period of the inverse relationship. That is

$$\tilde{r}_i(t) = \sum_{k=-\infty}^{\infty} R_i(k) e^{jk2\pi f_0 t}, \quad \text{for all } t$$

$$r_i(t) = \tilde{r}_i(t) \quad \text{for } 0 \leq t \leq T$$

For practical cases the $r_i(t)$ are bandlimited signals so that the Fourier coefficients are all zero outside some range, say, $-N \leq k \leq N$. We see then that the $r_i(t)$ can be characterized by the set of Fourier Series coefficients, $R_i(k)$, $-N \leq k \leq N$.

We wish to obtain an expression for the joint probability density function of these coefficients conditioned on a hypothesized value for the time delay, denoted by τ , which is chosen from the range of possible delays. As will be seen, the coefficients are also dependent upon the power spectral density functions of received signals, which, for now, we will assume are known.

First we observe from (2.6) that each coefficient $R_i(k)$, $i = 1, 2$, for any particular value of k in the range $-N \leq k \leq N$, is a zero mean Gaussian random variable. This is because it is derived by a linear transformation on the received signal $r_i(f)$, which, as we have assumed, is zero-mean Gaussian. So we have

$$E[R_1(k)] = 0 \quad -N \leq k \leq N$$

$$E[R_2(k)] = 0 \quad -N \leq k \leq N$$

For large T (i.e., small f_0)

$$E[R_1(k)R_2(j)^*] = \begin{cases} \frac{1}{T} G_{r_1 r_2}(kf_0) & \text{for } k = j \\ \sim 0 & \text{for } k \neq j \end{cases}$$

That is for large T , the coefficients are essentially uncorrelated.

We next form a bivariate Gaussian random column vector

$$\underline{R}(k) \triangleq [R_1(k), R_2(k)]'$$

for each value of k in $-N \leq k \leq N$ (the ' denotes the transpose of the vector). In order to represent its conditional density function, we need the covariance matrix

$$\text{COV}_{k|\tau} = \begin{bmatrix} \text{Cov}[R_1(k), R_1(k)] & \text{Cov}[R_1(k), R_2(k)] \\ \text{Cov}[R_2(k), R_1(k)] & \text{Cov}[R_2(k), R_2(k)] \end{bmatrix}$$

where $\text{Cov}(R_m, R_n)$ is the covariance of the random variables $R_m(k)$ and $R_n(k)$

$$\text{Cov}[R_m, R_n] = E[R_m(k)R_n(k)^* | \tau] - E[R_m(k) | \tau]E[R_n(k)^* | \tau]$$

Since the $R_i(k)$ are zero mean random variables

$$\text{Cov}[R_m, R_n] = E[R_m(k)R_n(k)^* | \tau]$$

which from (2.6) is

$$\text{Cov}[R_m(k), R_n(k)] = \frac{1}{T} G_{rm, rn}(kf_o)$$

Substituting into the covariance matrix:

$$\begin{aligned} \text{COV}_{k|\tau} &= \frac{1}{T} \begin{bmatrix} G_{r1r1}(kf_o) & G_{r1r2}(kf_o) \\ G_{r2r1}(kf_o)^* & G_{r2r2}(kf_o) \end{bmatrix} \\ &\triangleq \frac{1}{T} Q(k), \end{aligned} \quad (2.7)$$

where $Q(k)$ is referred to as the cross-spectral density matrix. For any particular value of k , $-N \leq k \leq N$, we now can write the bivariate Gaussian probability density function for $\underline{R}(k)$ conditioned on τ , in standard form:

$$p(\underline{R}(k)|\tau) = \left\{ 2\pi |\text{COV}_{k|\tau}|^{1/2} \right\}^{-1} \exp -1/2 \left\{ \underline{R}(k)^{*'} [\text{COV}_{k|\tau}]^{-1} \underline{R}(k) \right\}$$

We now wish to consider the conditional pdf of $\underline{R}(k)$ for all values of k , $-N \leq k \leq N$, considered jointly. To do this we define our observation vector as

$$\underline{R} \triangleq [\underline{R}(-N), \underline{R}(-N+1), \dots, \underline{R}(N)].$$

Now since the $\underline{R}(k)$'s are uncorrelated (and being Gaussian, also independent), the conditional joint pdf of \underline{R} is simply the product of the pdf's for each individual $\underline{R}(k)$:

$$p(\underline{R}|\tau) = \prod_{k=-N}^N p(\underline{R}(k)|\tau)$$

if we let:

$$c = \prod_{k=-N}^N (2\pi |\text{COV}_{k|\tau}|^{1/2})^{-1} \quad (2.8)$$

where $|\cdot|$ is the determinant, and

$$J_1 = \sum_{k=-N}^N \underline{R}(k)^{*'} [\text{COV}_{k|\tau}]^{-1} \underline{R}(k) \quad (2.9)$$

we can write $p(\underline{R}|\tau)$ in the simple form of

$$p(\underline{R}|\tau) = c \exp(-J_1/2) \quad (2.10)$$

Summarizing where we stand, we have an observation vector \underline{R} which is conditioned upon the possible values of the time delay, and is also dependent upon the power-spectra of the received data. The elements of our observation vector are the Fourier Series coefficients of $r_1(t)$ and $r_2(t)$. Now we will use a maximum à posteriori decision criterion and assume that all possible values of τ are equally likely (the actual range of possible values for τ is dependent upon the source/receiver geometry). Thus the maximum likelihood estimate for D (the actual time delay of interest), is to choose $\hat{D} = \tau$, where τ gives the maximum value for $p(\underline{R} | \tau)$. That is, we choose the τ that most likely would have given us the observed values in \underline{R} .

We will now use equations (2.7), (2.8), (2.9), and (2.10) and some simplifying approximations to reduce this test to equivalent ML tests until we get it in the final desired form.

First, we show that c is independent of τ , and thus can be dropped from the test. For uncorrelated noise, our model yields

$$G_{r1r1}(kf_o) = G_{ss}(kf_o) + G_{n1n1}(kf_o) \quad (2.11)$$

$$G_{r2r2}(kf_o) = \alpha^2 G_{ss}(kf_o) + G_{n2n2}(kf_o) \quad (2.12)$$

$$G_{r1r2}(kf_o) = \alpha G_{ss}(kf_o) e^{-jk2\pi f_o \tau} \quad (2.13)$$

(substituting the hypothesized delay, τ , for the true delay, D). Then the determinant of $\text{COV}_{k|\tau}$ in (2.8) is

$$\begin{aligned} \left| \text{COV}_{k|\tau} \right| &= [G_{ss}(kf_o) + G_{n1n1}(kf_o)] [\alpha^2 G_{ss}(kf_o) + G_{n2n2}(kf_o)] \\ &\quad - [\alpha G_{ss} e^{-jk2\pi f_o \tau}] [\alpha G_{ss} e^{+jk2\pi f_o \tau}] \end{aligned}$$

The exponentials in the last term cancel, so the determinant and thus c are independent of τ .

Next, we observe that the summand of (2.9) is ≥ 0 (positive semidefinite, [17, p. 182]). With this in mind and dropping the c term, the equivalent test is to choose τ which gives the minimum value for J_1 in (2.9).

We now make an approximation based on the relationship between the Fourier Series and the Fourier Transform. For large T and kf_o held constant, it can be shown [18, pp. 23-25]

$$J_1 = \int_{-\infty}^{\infty} \underline{R}(f)^* \underline{Q}^{-1}(f) \underline{R}(f) df \quad (2.14)$$

We next determine $\underline{Q}^{-1}(f)$ from (2.7), substitute into (2.14), and use (2.11), (2.12), (2.13) to obtain

$$J_1 = J_2 - J_3$$

where

$$J_2 = \int_{-\infty}^{\infty} \left[|R_1(f)|^2 / G_{r1r1}(f) + |R_2(f)|^2 / G_{r2r2}(f) \right] \cdot 1/[1 - C_{r1r2}(f)] df \quad (2.15)$$

$$J_3 = 2 \int_{-\infty}^{\infty} R_1(f) R_2(f)^* \frac{\alpha G_{ss}(f) e^{j2\pi f \tau}}{G_{r1r1}(f) G_{r2r2}(f) (1 - C_{r1r2}(f))} df \quad (2.16)$$

and

$$C_{r1r2}(f) \triangleq \frac{|G_{r1r2}(f)|^2}{G_{r1r1}(f)G_{r2r2}(f)} \quad (2.17)$$

is the magnitude squared coherence [19, p. 54] which is bounded by -1 and 1.

Since J_2 is not dependent on τ , the ML estimate reduces to picking τ which maximizes J_3 .

If the $R_1(f)R_2(f)^*$ term in (2.16) is computed for the interval $0 \rightarrow T$ by averaging short segments, then it can be viewed as being equal to T times an estimate of the cross-power spectrum, $T \hat{G}_{r1r2}(f)$. We can rewrite J_3 as

$$J_3 = 2T\alpha \int_{-\infty}^{\infty} \hat{G}_{r1r2}(f) \cdot \frac{G_{ss}(f) e^{j2\pi f\tau}}{G_{r1r1}(f)G_{r2r2}(f) (1-C_{r1r2}(f))} df \quad (2.18)$$

but, using (2.11), (2.12), (2.13) and (2.17)

$$\begin{aligned} \frac{G_{ss}(f)}{G_{r1r1}(f)G_{r2r2}(f)} &= \frac{|G_{r1r2}(f)|}{G_{r1r1}(f)G_{r2r2}(f)} \\ &= \frac{|G_{r1r2}(f)|}{|G_{r1r2}(f)|} \cdot \frac{|G_{r1r2}(f)|}{G_{r1r1}(f)G_{r2r2}(f)} \end{aligned}$$

$$= \frac{C_{r1r2}(f)}{|G_{r1r2}(f)|} \quad (2.19)$$

Substituting (2.19) into (2.18) and dropping the $2T\alpha$ constant, we get our ML estimator in our final form, that is a Generalized Cross-Correlation (GCC)

$$R_{r1r2}^{ML}(\tau) = \int_{-\infty}^{\infty} \hat{G}_{r1r2}(f) \frac{1}{|G_{r1r2}(f)|} \frac{C_{r1r2}(f)}{[1 - C_{r1r2}(f)]} e^{j2\pi f\tau} df \quad (2.20)$$

Summarizing, our ML estimate reduces to picking as our estimate of the time delay D , the value of τ which maximizes the GCC. The GCC is computed by taking the inverse Fourier Transform of a weighted estimate of the cross-power spectrum of the two received signals $r_1(t)$ and $r_2(t)$. The ML weighting is

$$W^{ML}(f) = \frac{1}{|G_{r1r2}(f)|} \frac{C_{r1r2}(f)}{[1 - C_{r1r2}(f)]} \quad (2.21)$$

which is defined as long as either or both $G_{n1n1}(f)$ and $G_{n2n2}(f)$ are non-zero and independent (thus $C_{r1r2}(f) < 1$), as would be the case in practice.

Up to this point, we have assumed that the signal and noise auto- and cross-spectra were known. In practice they may have to be estimated by any of various techniques (see

for example [19], [20], [21], [22], and [23]). In such case the ML estimator is only approximately achieved.

We now will very briefly show that this ML estimator has a variance which is equal to the minimum bound on the variance, and as such is optimum.

Carter and Knapp [7] indicate that by using results obtained from [24], the variance of a time delay estimate which is in the region of the true delay (i.e., small estimation error) and using any general weighting, $W(f)$, is

$$\text{Var}[\hat{D}] = \frac{\int_{-\infty}^{\infty} W(f)^2 (2\pi f)^2 G_{r1r1}(f) G_{r2r2}(f) [1 - C_{r1r2}(f)] df}{[T \int_{-\infty}^{\infty} (2\pi f)^2 |G_{r1r2}(f)| W(f) df]^2} \quad (2.22)$$

If we substitute $W^{\text{ML}}(f)$ from (2.21), make use of the definition of $C_{r1r2}(f)$ from (2.17), and consider the frequency symmetry of the magnitude of the cross-spectrum, (2.22) reduces to

$$\text{Var}[\hat{D}] = \left[2T \int_0^{\infty} (2\pi f)^2 \frac{C_{r1r2}(f)}{1 - C_{r1r2}(f)} df \right]^{-1} \quad (2.23)$$

We now show that this is the minimum variance. The Cramér-Rao Lower Bound (CRLB) on the variance is [25, p. 72]:

$$\text{Var}[\hat{D}] \geq - \left[E \left\{ \frac{\partial^2 \ln p(R(k)|Q, \tau)}{\partial \tau^2} \right\} \right]^{-1} \Big|_{\tau = D}$$

Since, for the ML estimator, the only part that is dependent on τ is J_3 , then we can write

$$\text{Var}[\hat{D}] \geq - \left[\frac{\partial^2}{\partial \tau^2} E (J_3/2) \right]^{-1}$$

Since

$$G_{r1r2}(f) = G_{r1r2}(f) e^{-j2\pi fD}$$

and

$$E[\hat{G}_{r1r2}(f)] = G_{r1r2}(f),$$

we have

$$E [J_3/2] = T \int_{-\infty}^{\infty} e^{+j2\pi f(\tau-D)} \cdot \frac{C_{r1r2}(f)}{1-C_{r1r2}(f)} df$$

Then the minimum variance is

$$\text{Min Var}[\hat{D}] = \left[T \int_{-\infty}^{\infty} (2\pi f)^2 \frac{C_{r1r2}(f)}{1-C_{r1r2}(f)} df \right]^{-1}$$

comparing this with (2.23) and considering the symmetry of $C_{r1r2}(f)$ we see that the GCC attains this minimum variance.

2.3 Performance of the GCC Time Delay Estimator

The variance of the TDE by the GCC method (2.23), as mentioned earlier, achieves the Cramér-Rao Lower Bound (CRLB) of the estimator variance. In the form of (2.23), it is somewhat difficult to interpret directly the effects of such important parameters like signal and noise bandwidth and SNR. Quazi [26] gives several forms which are more useful for such interpretation.

If the autospectra of the signal and noise are assumed to have the same shape (i.e., SNR constant), over the band f_1 to f_2 Hz, it is easy to show that the CRLB is

$$\text{CRLB} = \frac{3}{8\pi^2 T} \cdot \frac{1+2\text{SNR}}{\text{SNR}^2} \cdot \frac{1}{f_2^3 - f_1^3} \quad (2.24)$$

If $\text{SNR} \ll 1$ then

$$\text{CRLB} \cong \frac{3}{8\pi^2 T} \cdot \frac{1}{\text{SNR}^2} \cdot \frac{1}{f_2^3 - f_1^3} \quad (2.25)$$

This can be expressed in terms of signal and noise bandwidth $W = f_2 - f_1$, and center frequency $f_0 = (f_1 + f_2)/2$, as (for $\text{SNR} \ll 1$):

$$\text{CRLB} \cong \frac{1}{8\pi^2} \cdot \frac{1}{\text{SNR}^2} \cdot \frac{1}{TW} \cdot \frac{1}{f_0} \cdot \frac{1}{1+(W^2/12f_0^3)}.$$

for $\text{SNR} \gg 1$

$$\text{CRLB} \cong \frac{3}{4\pi^2 T} \cdot \frac{1}{\text{SNR}} \cdot \frac{1}{f_2^3 - f_1^3}$$

or

$$\text{CRLB} \cong \frac{1}{4\pi^2} \cdot \frac{1}{\text{SNR}} \cdot \frac{1}{TW} \cdot \frac{1}{f_0} \cdot \frac{1}{1+(W^2/2f_0)}.$$

From the above representations, it is seen that CRLB varies inversely as the time-bandwidth product, TW . For $W \ll f_0$, it varies inversely as the center frequency, f_0 . And at low SNR's, it varies inversely as the SNR^2 , while at high SNR's, it varies inversely as SNR. Finally, an important relationship is that for a given SNR, W , and f_0 , the variance varies inversely as the total observation time T .

The CRLB gives actual achievable performance for the GCC if erroneous estimates are in the region of the true correlation peak. If there is insufficient observation time for a given SNR and bandwidth, then large anomalous peaks can occur far from the true delay region which results in large estimation errors. In this situation, the performance of the estimator will be significantly worse than the CRLB. Figure 6 illustrates this effect for a low pass filtered signal. The top plot shows what an ideal correlation would look like for no noise present and very long observation time. For the realistic case of moderate noise present, the center figure is more representative. The correlation peaks occur away from the true delay, but are still in the general

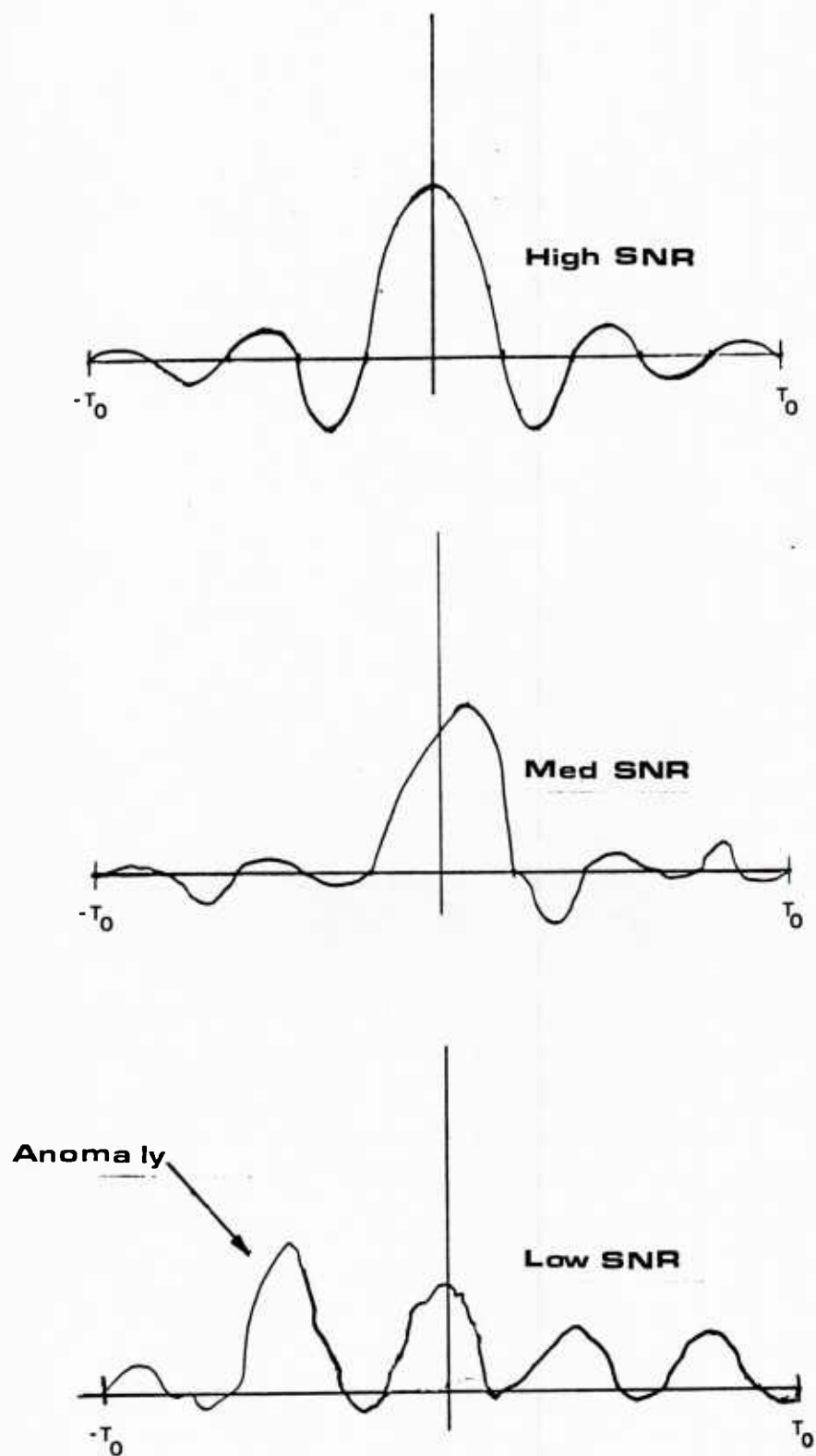


FIGURE 6
ANOMALOUS PEAKS IN THE CROSS-CORRELATION FUNCTION

neighborhood. In this situation the CRLB gives a good estimate of actual performance, i.e., it is a "tight" bound. As the SNR is decreased further, a point is reached where large peaks (referred to as anomalies [27]) occur far from the region of the true value of the time delay. In this situation, the performance deviates significantly (gets worse) from the CRLB, and it is no longer a tight bound.

Recent work by Ianniello, Weinstein and Weiss has dealt with determining a tighter bound than the CRLB at these lower SNR's [28], [29], [30], [31]. Ianniello [29] has derived a performance estimator (not a bound in the strict sense), which has been called the Correlation Performance Estimate (CPE) [32], for the GCC. It is shown to be

$$\text{Var}[\hat{D}]_{\text{CPE}} = PT_0/3 + (1-P)\text{Var}[\hat{D}]_{\text{CRLB}} \quad (2.26)$$

T_0 is the correlation peak search window, i.e., if we know a priori that the maximum possible value of τ is $\pm T_0$ then we search for peaks only in this region of the cross-correlation function (for example if we know the sensor separation, L , we know the maximum delay between them is $T_0 = \pm L/c$, c = speed of sound). The probability that an anomalous noise peak occurs (i.e., the maximum correlation peak in $-T_0 \leq \tau \leq T_0$ occurs "far" from the true delay) is P . This probability is shown to be:

$$P \cong 1 - \int_{-\infty}^{\infty} \frac{1}{2\pi} \exp[-(x-K_1)^2/2] dx \left[\int_{-\infty}^{Zx} (1/2\pi) \exp(-y^2/2) dy \right]^{M-1}$$

$$\text{where: } K_1 = \frac{\sqrt{B_s T} (\text{SNR})}{[(\text{SNR})^2 + (1+\text{SNR})^2]^{1/2}}$$

$$Z = \left[1 + \frac{\text{SNR}^2}{(1+\text{SNR})^2} \right]^{1/2}$$

$$M = 4BT_o \text{ (for uniform spectra over } -B \leq f \leq B)$$

$$= \# \text{ independent values of } \hat{R}_{y1y2}(\tau) \text{ in } -T_o \leq \tau \leq T_o$$

and B_s is the statistical bandwidth ($B_s = 2B$ for flat spectrum, low-pass signal and noise). Uncorrelated zero-mean Gaussian signal and noise are assumed. One can evaluate P numerically [13].

From (2.26), we see that if $P = 0$ then we just have the CRLB. If $P = 1$, then we have the variance of a uniformly distributed random variable, ranging between $\pm T_o$, as might be expected, since at very low SNR's, $P \rightarrow 1$, and the peak can occur anywhere, with equal likelihood, in the $\pm T_o$ peak search region.

Scarbrough, Tremblay and Carter [32], have done computer simulations which substantiate these results and extend them to make some observations regarding the significance of TDE processing by coherent vs. incoherent means. Figure 7 shows a typical comparison of the CRLB and the CPE performance plots. (Note that the vertical axis is in \log_{10} of the standard deviation of \hat{D} , $\text{Std}[\hat{D}]$, not the variance. In this case signal and noise are low-pass filtered, flat spectrum, Gaussian processes, both with

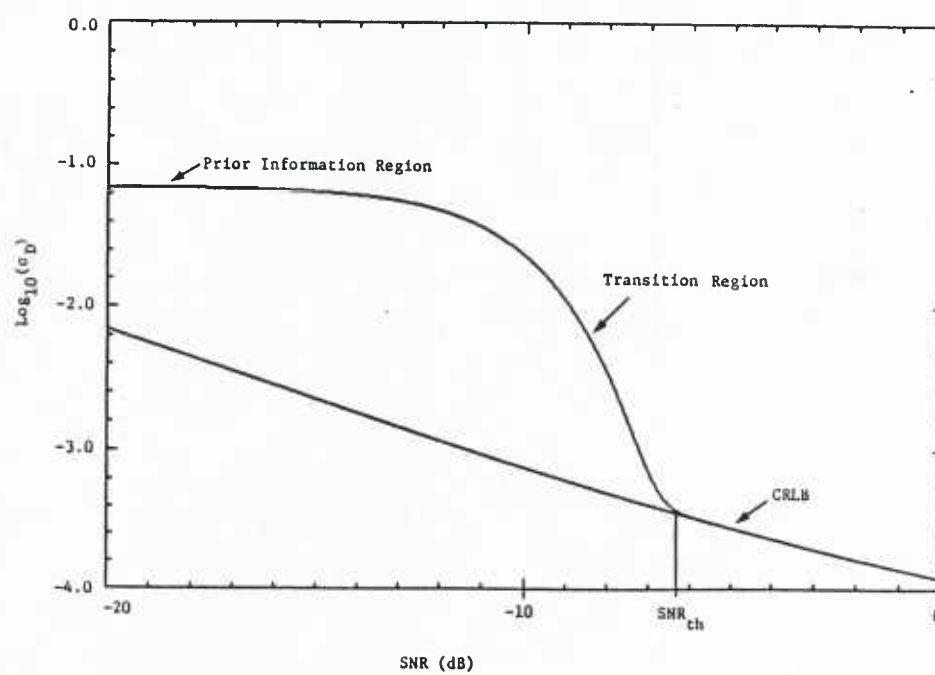


FIGURE 7
CPE vs. CRLB

bandwidth, $B = 100$ Hz, integration time, $T = 8$ secs, and correlation search peak windows of $T_0 = \pm 1/8$ sec. The estimator is seen to achieve the CRLB for $\text{SNR} \geq 6\text{dB}$. As the SNR is lowered, performance rapidly starts to deviate away from the CRLB, first through a transition region, then finally into the region where the delay estimate becomes uniformly random across the peak search window, $\pm T_0$. Figure 8 is a family of curves for various integration times and fixed bandwidth and T_0 . As the integration time is increased the threshold SNR gets lower. Observe that for fixed B and T_0 , the value of $\log_{10} \text{Stdv}[D]$ at the various threshold SNR's is nearly constant. (Some further discussion on this is given in [13] and [33]). Figure 9 shows the results of the computer simulation done in [32], for two integration times (the X's and O's are the simulation data points overlayed on the calculated CPE's and CRLB's).

Figure 10 addresses the implications regarding coherent vs. incoherent TDE processing. The top curve, labeled "CPE (T=2)", is the CPE for a total integration time of 2 seconds. If 4 of these delay estimates are averaged to get a new estimate, the new estimate will have a reduced variance equal to $1/4$ that achieved by 2 second estimations. This process is referred to as "incoherent" processing and its expected performance is the curve labeled "CPE (T=8, N=4) (incoherent)". If, on the other hand, the full 8 seconds of data was processed coherently as one long correlation (or equivalently, coherently averaged consecutive correlation functions from contiguous, equal-sized partitions of the 8 second data), the performance obtained is the curve labeled "CPE (T=8)". We see that at higher SNR's the 8 second incoherent processing

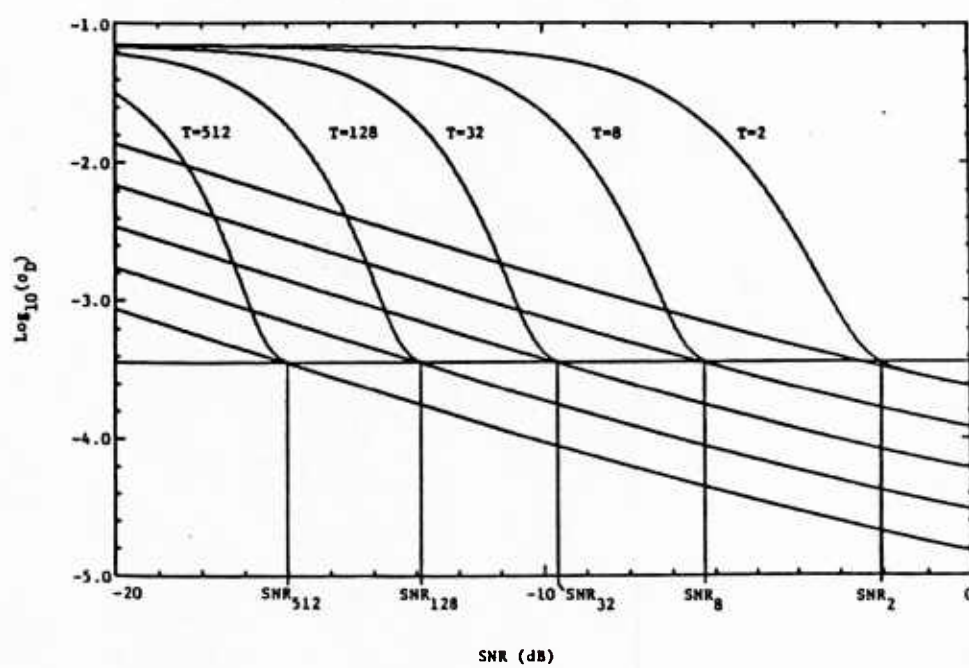


FIGURE 8
CPE AND CRLB FOR VARIOUS INTEGRATION TIMES

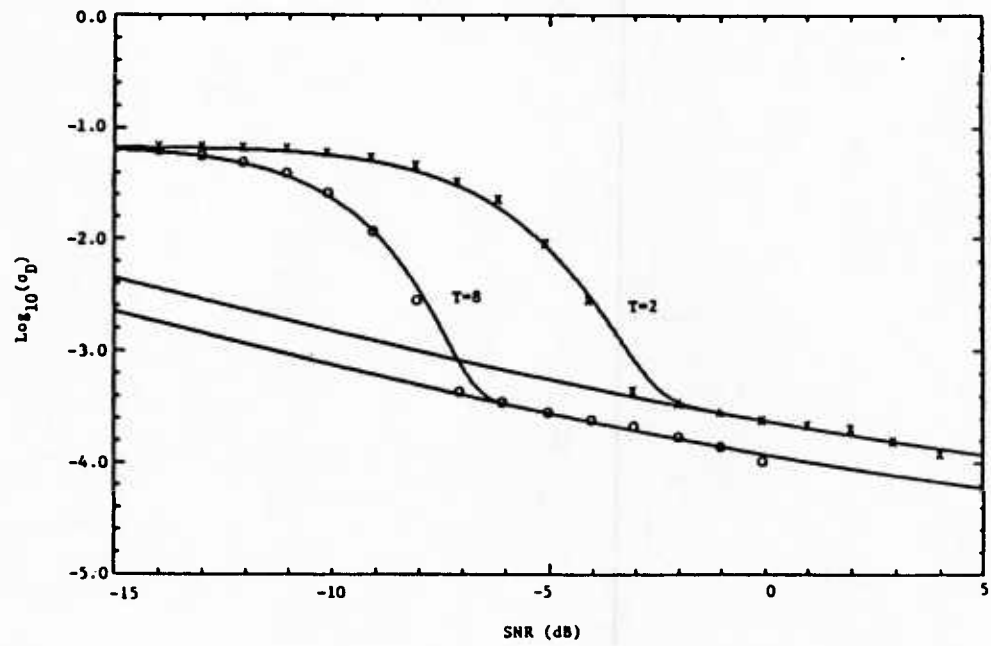


FIGURE 9
CPE AND CRLB VS. SIMULATION RESULTS

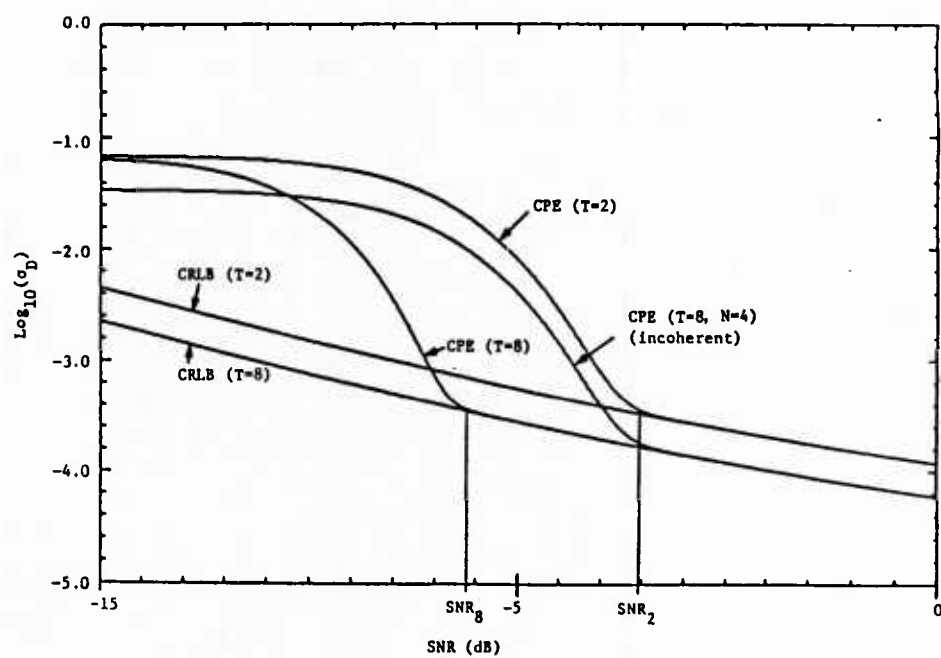


FIGURE 10
COHERENT AND INCOHERENT INTEGRATION PERFORMANCE

achieves the CRLB for $T=8$ seconds, but begins to deviate at SNR_2 , the threshold SNR for 2 second averaging. But, the 8 second coherent processor achieves the 8 second CRLB down to SNR_8 , the 8 second threshold SNR which for this case is $>4\text{dB}$ lower than SNR_2 . Thus, coherent processing is optimum at lower SNR's than the incoherent method, given the same amount of data.

3. TIME DELAY ESTIMATION WITH MOVING SOURCE AND/OR RECEIVERS

We have seen that the TDE correlator performance losses due to decreasing signal-to-noise ratio (SNR) can be regained to near CRLB performance by increasing the coherent integration time, T . For source and receivers with fixed relative positions, the GCC can be used without modification, other than to increase the total integration time (e.g. by taking longer segments or increasing the total number of segments processed). However, when the relative motion between the source and receivers is different for each of the receivers, the time-delay of arrival varies over T . This results in a loss of coherence between the 2 received signals which worsens as T gets longer, effecting a "smearing" of the correlation peak and a drop in it's amplitude which in turn can cause a significant increase in error. This is especially true if the delay varies by more than the correlation time width of the source signal during the $[0 \rightarrow T]$ observation time [34]. In order to get improved performance, one must compensate for this varying time delay to again allow longer integration time and use of the GCC processor. This section addresses this problem and some approaches to resolving it.

3.1 Motion Model

The model presented here is based on the one given by Knapp and Carter [35]. Other versions, which are equivalent but whose form offer additional insight to the problem are presented in [34], [36], [13], and [38]. The form of the model in [13] is primarily used in this section.

We let $s'(t)$ be the signal received at receiver 1 when no relative motion or noise is present. Then, for the case with relative motion and additive noise, an appropriate model would be

$$r_1(t) = s'(\beta_1 t) + n_1(t) \quad (3.1.a)$$

$$r_2(t) = \alpha s'(\beta_2(t+D)) + n_2(t) \quad (3.1.b)$$

The functions $r_1(t)$ and $r_2(t)$ are the receiver 1 and 2 inputs having stationary, white, zero-mean additive noise $n_1(t)$ and $n_2(t)$, which are uncorrelated with each other and $s'(t)$. The time delay, D , is the time difference of arrival (TDOA) as in the no motion model, and α is the attenuation of the signal at receiver 2 relative to that at receiver 1 (in most cases of interest, $\alpha \approx 1$). The relative motion between the source and each of the receivers causes a time compression/expansion, termed "time companding," [35] which, in general, is different for each receiver, and is represented by β_1 and β_2 . For relative velocity v_i between the source and receiver i , and signal propagation velocity, c , then

$$\beta_1 = 1 + v_1/c$$

$$\beta_2 = 1 + v_2/c$$

For acoustic sources in the ocean, $c \approx 4900$ feet/second and generally $c \gg v_i$, so $\beta_i \approx 1$. If a positive velocity v_i is assigned to source and receiver motion towards each other, then $\beta_i > 1$. It can be seen that the model in (3.1) reduces to the no motion model for $\beta_1 = \beta_2 = 1$. An important assumption made is that β_1 and β_2 are essentially constant

over the correlation time $0 \rightarrow T$ (i.e., accelerations in source/receiver positions are ignored).

A slightly different representation of the model will give a little added insight to the problem.

Let $s(t) = s'(\beta_1 t)$. Then

$$s'(t) = s(t/\beta_1)$$

$$s'(\beta_2(t+D)) = s([\beta_2/\beta_1](t+D))$$

Now let

$$\beta = \beta_2/\beta_1$$

then we can write (3.1) as

$$r_1(t) = s(t) + n_1(t) \quad (3.2.a)$$

$$r_2(t) = \alpha s(\beta(t+D)) + n_2(t) \quad (3.2.b)$$

In this form we see that the motion effects can be thought of in terms of a relative time companding (RTC), [35], [38], of the signal at receiver 2 with respect to that at receiver 1.

In yet another form, the motion effects can be seen as a time-varying time delay. From (3.2.b):

$$\begin{aligned}
s(\beta(t+D)) &= s(\beta t + \beta D) \\
&= s(t - t + \beta t + \beta D) \\
&= s(t + (\beta - 1)t + \beta D)
\end{aligned} \tag{3.3}$$

Define:

$$\begin{aligned}
d' &\triangleq (\beta - 1) \\
d_0 &\triangleq \beta D \\
d(t) &\triangleq d't + d_0
\end{aligned} \tag{3.4}$$

then

$$\begin{aligned}
s(\beta(t+D)) &= s(t + d't + d_0) \\
&= s(t + d(t))
\end{aligned}$$

and our model can now be written as:

$$r_1(t) = s(t) + n_1(t) \tag{3.5.a}$$

$$r_2(t) = \alpha s(t + d(t)) + n_2(t) \tag{3.5.b}$$

where $d(t)$ is seen to be a linearly time-varying delay with rate, d' , and initial value, d_0 . The two representations of the motion model in (3.2) and (3.5) point to two methods for compensating for motion effects. The first indicates a need to compensate by processing the receiver 2 inputs with a time compander that negates the time-companding due to motion and reverts back to the no motion case. The second form indicates compensation by removal of the time-varying

time delay effects. These approaches are discussed in the next two sections.

3.2 Compensating for Relative Time Companding

From (3.2) it is apparent that the effect of relative time companding may be removed by passing $r_2(t)$ through a time-compander which will perform time-scaling that is the inverse of β , i.e. generate

$$r_3(t) = r_2(t/b) \quad (3.6)$$

where $b = \beta$, ideally. Then $r_1(t)$ and $r_3(t)$ can be processed with the GCC as in the no-motion case.

By an argument very similar to that used to derive the GCC as a ML estimator, Knapp and Carter [35] show that the ML estimator when motion is present (at least to a reasonable approximation when the power spectra are unknown), is to maximize

$$J(\tau, b) = \int_{-\infty}^{\infty} R_1(f) R_3(f, b) \hat{W}^*(f, b) e^{j2\pi f \tau b} df \quad (3.7)$$

where τ and b are hypothesized values for D and β respectively, $R_1(f)$ and $\hat{R}_3(f, b)$ are the Fourier Transforms of $r_1(t)$ and $r_3(t)$, and $W(f, b)$ is the ML weighting function derived from estimates of the auto- and cross-power spectra of $r_1(t)$ and $r_3(t)$, defined as

$$\hat{W}(f, b) = \frac{\hat{C}_{r_1 r_3}(f, b)}{\left| \hat{G}_{r_1 r_3}(f, b) \right| (1 - \hat{C}_{r_1 r_3}(f, b))} \quad (3.8)$$

and $\hat{C}_{r_1 r_3}(f, b)$ is the magnitude squared coherence estimate:

$$\hat{C}(f, b) = \frac{|\hat{G}_{r_1 r_3}(f, b)|^2}{\hat{G}_{r_1 r_1}(f) \hat{G}_{r_3 r_3}(f, b)} \quad (3.9)$$

Note that except for the dependencies on b due to the hypothesized compensation of $r_2(t)$ the above are the same form as for the GCC. Then $J(\tau, b)$ can be seen to be a correlation function with argument τb , which if $\tau = D$ and $b = \beta$ is $D\beta = d_0$.

The compensation for time-companding must be done for a range of hypothesized b 's, then each $J(\tau, b)$ is computed as in (3.7) giving a two-dimensional ambiguity surface in τ and b space. The global peak on this surface is found and it's corresponding values of τ and β are our ML estimates of D and β respectively. Figure 11 illustrates this process. The $COMP_i$, $i = 1$ to N_c , represents compensation for time-companding using one of N_c hypothesized values for b .

The preceding process is quite expensive computationally. The entire GCC process must be done for each hypothesized b , including calculation of $\hat{W}(f, b)$. The compensating companding processor could involve hardware such as a variable speed analog tape recorder or multiple rate samplers to effect the time compression/expansion of $r_2(f)$. Or it could be done in software with a very fine resolution interpolation algorithm followed by variable rate re-sampling. Although any of these methods are feasible (Betz has implemented the latter technique and found it to perform near optimum [39]), it would be desirable to find a more efficient way to compensate for the effects of relative motion. As will be seen in the next section, this can be

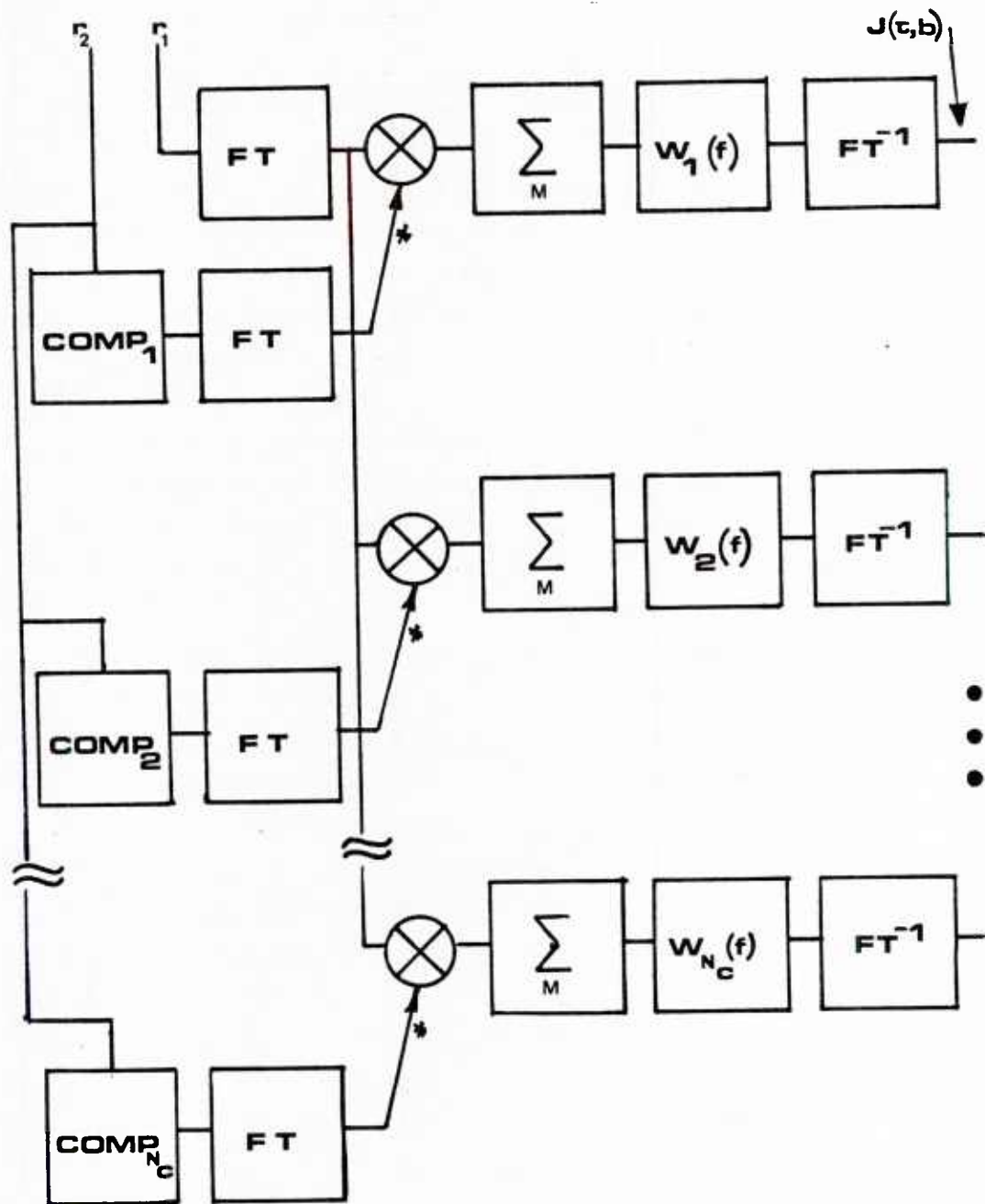


FIGURE 11
TIME-COMPANDING BLOCK DIAGRAM

done if we compensate for the varying time-delay of (3.5) instead of the relative time companding of (3.2).

3.3 Compensating for Varying Time-Delay

The general strategy that will be used to compensate for the linearly time-varying delay indicated in (3.4) and (3.5) can be summarized briefly as follows. The total coherent processing interval from $t = 0$ to T seconds, is divided into several equal-sized, short-time intervals. Assuming that the delay change during each short-time interval is relatively small, a modified model is formed by approximating the continuously changing delay during each short-time interval as a constant equal to the actual delay at the mid-point of that interval. Then, based on this model, the compensation is done in a step-wise fashion for each short-time interval, by adjusting for the amount of delay change from interval to interval. A compensated short-time GCC type cross-correlation function is computed for each interval. These are then averaged to get a total coherent processing time of T seconds. The above is done for a range of assumed delay rates, forming an ambiguity surface from which the ML delay and delay rate are determined. This process closely approximates the ML method of relative time-companding compensation of Section 3.2, but without the need of performing time-scaling. Also, only one weighting function, $W(f)$, needs to be computed since there is no dependency on an assumed time-scaling factor, b , as was the case in the time-companding compensation method.

This piecemeal approach to removing the effects of varying time-delay can be implemented in two ways, as described in [36] and, more recently, by [13], [37] and

[38]. The effect of this process has been described as "deskewing" in [38] for reasons that will be apparent shortly.

From (3.5) we can write the cross-correlation function of $r_1(t)$ and $r_2(t)$ at times t_1 and t_2 as:

$$\begin{aligned} R_{r_1 r_2}(t_1, t_2) &= E[r_1(t_1) r_2(t_2)] \\ &= E \left\{ [s(t_1) + n_1(t_1)] [\alpha s(t_2 + d(t_2)) + n_2(t_2)] \right\} \end{aligned}$$

Since $s(t)$, $n_1(t)$ and $n_2(t)$ are zero-mean and mutually uncorrelated, we have

$$R_{r_1 r_2}(t_1, t_2) = \alpha E[s(t_1) s(t_2 + d(t_2))].$$

Letting $t_1 = t + \tau$ and $t_2 = t$,

$$\begin{aligned} R_{r_1 r_2}(t + \tau, t) &= \alpha E[s(t + \tau) s(t + d(t))] \\ &= \alpha R_{ss}(t + \tau, t + d(t)) \end{aligned}$$

Since $s(t)$ is wide sense stationary, its auto-correlation function is dependent only on the difference of its time arguments, so

$$\begin{aligned} R_{r_1 r_2}(t + \tau, t) &= \alpha R_{ss}(\tau - d(t)) \\ &= \alpha R_{ss}(\tau - d' t - d_0) \end{aligned} \tag{3.10}$$

We see that the cross-correlation function is dependent on t , so, clearly, $r_1(t)$ and $r_2(t)$ are jointly non-stationary.

Our next step will be to break up the desired coherent processing time, $t = 0 \rightarrow T$, into M equal-sized short time intervals and label them T_k where

$$T_k = \left\{ t \mid (k-1)T/M \leq t \leq kT/M \right\}, \quad k = 1, 2, \dots, M$$

It is desired to make these intervals short enough so that the amount of change in the delay, $d(t)$, is small compared to the change over the entire interval. Yet, they should be long enough to assure independent correlations for each interval. Betz [38] has numerically determined an upper bound on the number of segments to be

$$M \leq WT/3.5$$

for low-pass, white signal and noise.

Next, we approximate the continuous, linearly varying time delay, $d(t)$, in a piece-wise constant fashion by using its values at the midpoint of each interval, T_k , [13], [36], [38]. The value of t at such midpoints is denoted

$$t_k = (k-1/2)T/M$$

and the value of the delay at the midpoint is

$$\begin{aligned} d(t_k) &= d't_k + d_o \\ &= d_k + d_o \end{aligned} \tag{3.11}$$

where $d_k \triangleq d't_k$. This is illustrated in Figure 12.

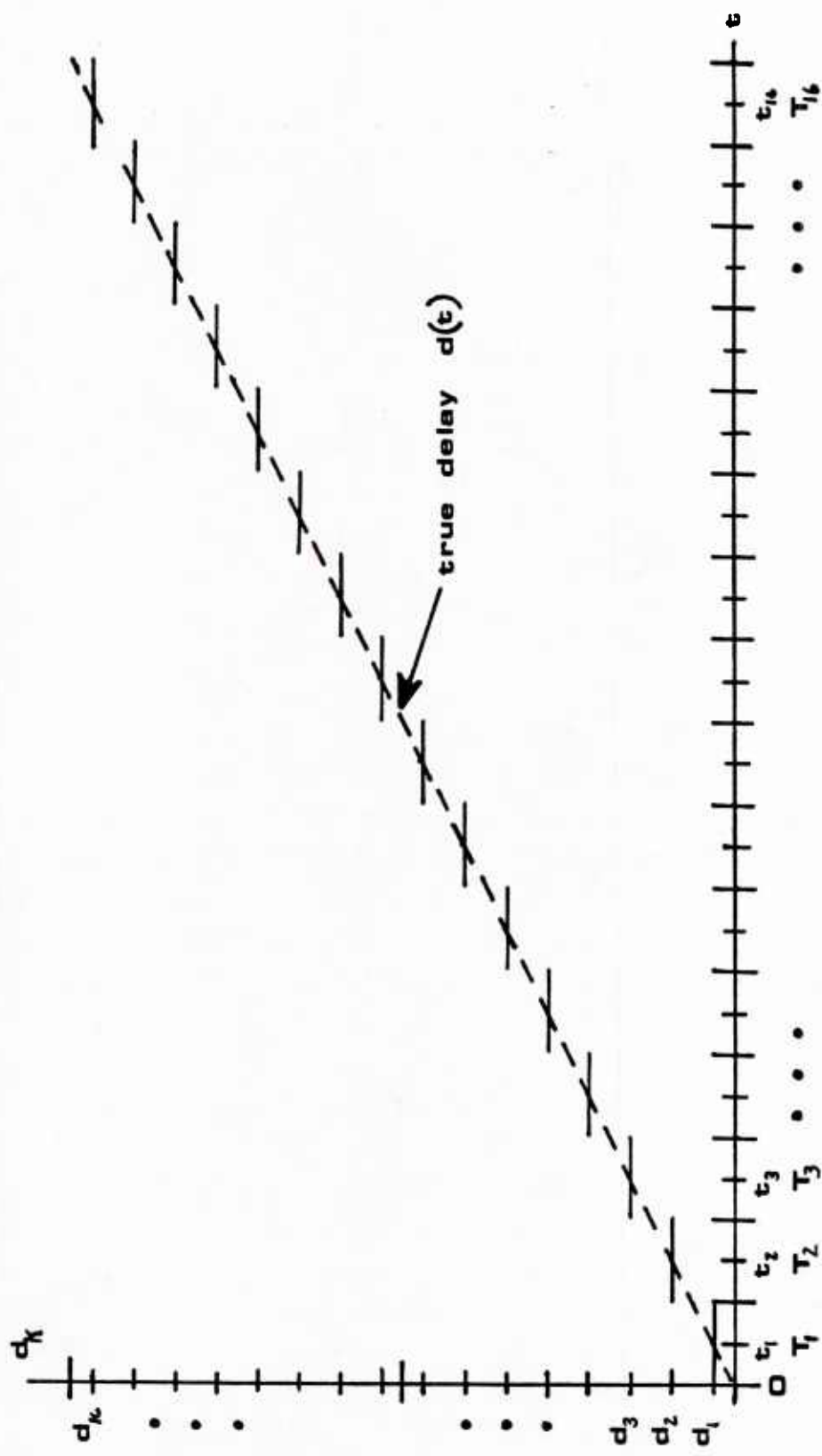


FIGURE 12
STEP-WISE CONSTANT APPROXIMATION OF DELAY RATE

Substituting (3.11) into (3.10) gives the approximate short-time cross-correlation function for each interval T_k as

$$R_{r1r1}(\tau, k) = \alpha R_{ss}(\tau - d_k - d_o) \quad (3.12)$$

which now is wide sense stationary (independent of t) within the k^{th} interval. In this form, we can envision that over the total observation time, $t = 0 \rightarrow T$, that the short term cross-correlation functions are approximately equal to short-time auto-correlation functions of the signal which is initially shifted in delay by d_o , and subsequently shifted (or "skewed") in τ by the amount d_k during each following short-time interval. Figure 13 is an actual set of these short-time cross-correlations generated by the simulation program described in Appendix A, which illustrates this skewing effect for $d_o = 0, d' = 1/256$, and $\text{SNR} = +6\text{dB}$. The plots show an expanded region around ± 50 sample intervals. It should be clear from the figure that if these correlations are simply averaged, without compensating for the skewness, that the resulting cross-correlation function will be smeared, as shown in Figure 14. This smearing leads to a broadening of the correlation peak and a reduction in its mean value [34], [36], [38]. This can be expected to increase the uncertainty of the true peak location and susceptibility to random noise effects, resulting in an increase in the variance of the delay estimate. Another effect is to cause a bias in the delay estimate towards the value of the true delay at time $T/2$ [35]. So our intent is to compensate by realigning or "deskewing" [38] the correlation functions with respect to that of the beginning of the T_1 interval before summing, in order to get the maximum benefit of the averaging process in reducing noise.

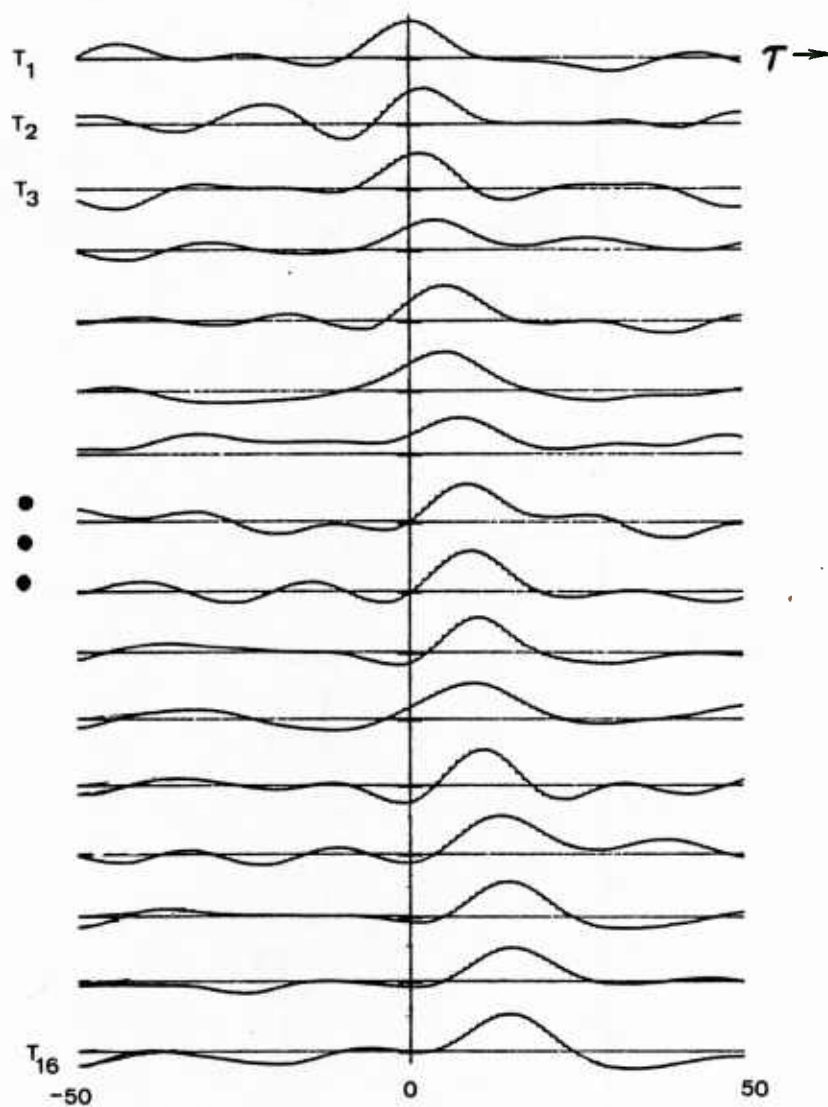


FIGURE 13
UNCOMPENSATED SHORT-TIME CROSS-CORRELATION
FUNCTIONS (UNAVERAGED)

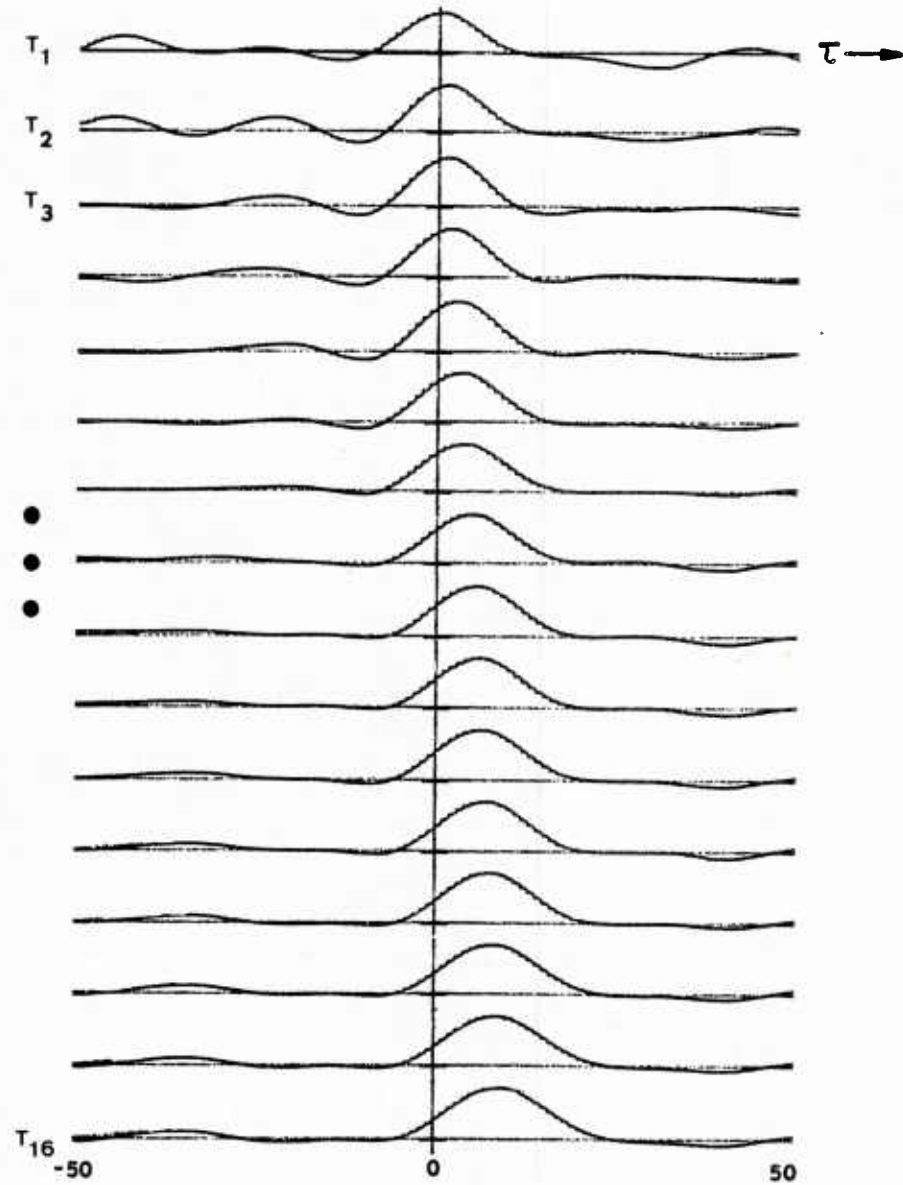


FIGURE 14
UNCOMPENSATED SHORT-TIME CROSS-CORRELATION
FUNCTIONS (AVERAGED)

As will be seen next, this deskewing can be done as a phase rotation of the short-time cross-spectra in the frequency domain, or as a delay shift in the time-delay domain. The first method has been implemented by Kuhn, Robison, and Winfield [36], by Scarbrough [13], and is the method used in the simulations done for this thesis, described in Section 4.0 and Appendix A. The latter method has been implemented by Betz [38], and termed "Deskewed Short-Time Correlation," an name which could be appropriate for either approach, as the net effect is essentially the same.

3.3.1 Compensation in the Frequency Domain (Phase Rotation)

We proceed by taking the Fourier Transform of (3.12) to get

$$G_{r1r2}(f,k) = \alpha G_{ss}(f) e^{-j2\pi f(d_k + d_o)}$$

It is clear that the time-varying delay is equivalent to a corresponding time-varying phase rotation of the signal auto-power spectrum by an amount $(-2\pi f d_k)$ radians. We can compensate for this with a counter rotation, $+ 2\pi f \hat{d}_k$, where

$$\hat{d}_k = \tau' t_k$$

is the amount of delay shift at time t_k (since $t = 0$); τ' is an hypothesized delay rate (and so an estimate of the true rate, d'), chosen from a range of possible delay rates. Then, averaging the compensated short-time cross-spectra:

$$\begin{aligned}\hat{G}_{r1r2}(f, \tau) &= (1/M) \sum_{k=1}^M \hat{G}_{r1r2}(f, k) e^{+j2\pi(\tau' t_k)} \quad (3.13) \\ &\cong (1/M) \sum_{k=1}^M \alpha G_{ss}(f, k) e^{-j2\pi f(d_k - \hat{d}_k + d_0)}\end{aligned}$$

If we hypothesize τ' , and thus, \hat{d}_k , correctly then

$$\hat{G}_{r1r1}(f) = \alpha G_{ss}(f) e^{-j2\pi f d_0}$$

This is the same cross-spectrum used in the GCC estimator (2.20), so that after delay rate compensation the no-motion GCC processing (i.e. ML weighting and inverse Fourier Transform) can be used to estimate the delay for a range of hypothesized τ' . The resultant two-dimensional (τ, τ') ambiguity surface is searched for the global maximum peak. The corresponding value of τ and τ' are our ML estimates for d' and d_0 respectively. This process is illustrated in Figure 15.

3.3.2 Compensation in the Delay (Deskewing)

In this approach, the individual cross-spectra from each short-time interval is weighted by $w^{ML}(f)$ and inverse Fourier Transformed to get M short-time cross-correlation functions. Each of these is progressively skewed in the delay dimension, as in Figure 13. Then each short-time correlation function for the interval T_k is shifted (deskewed) by $\hat{d}_k = \tau' t_k$. This is done, for example, by interpolation with a cubic spline as in [38]. Finally the deskewed cross-correlations are averaged to get the

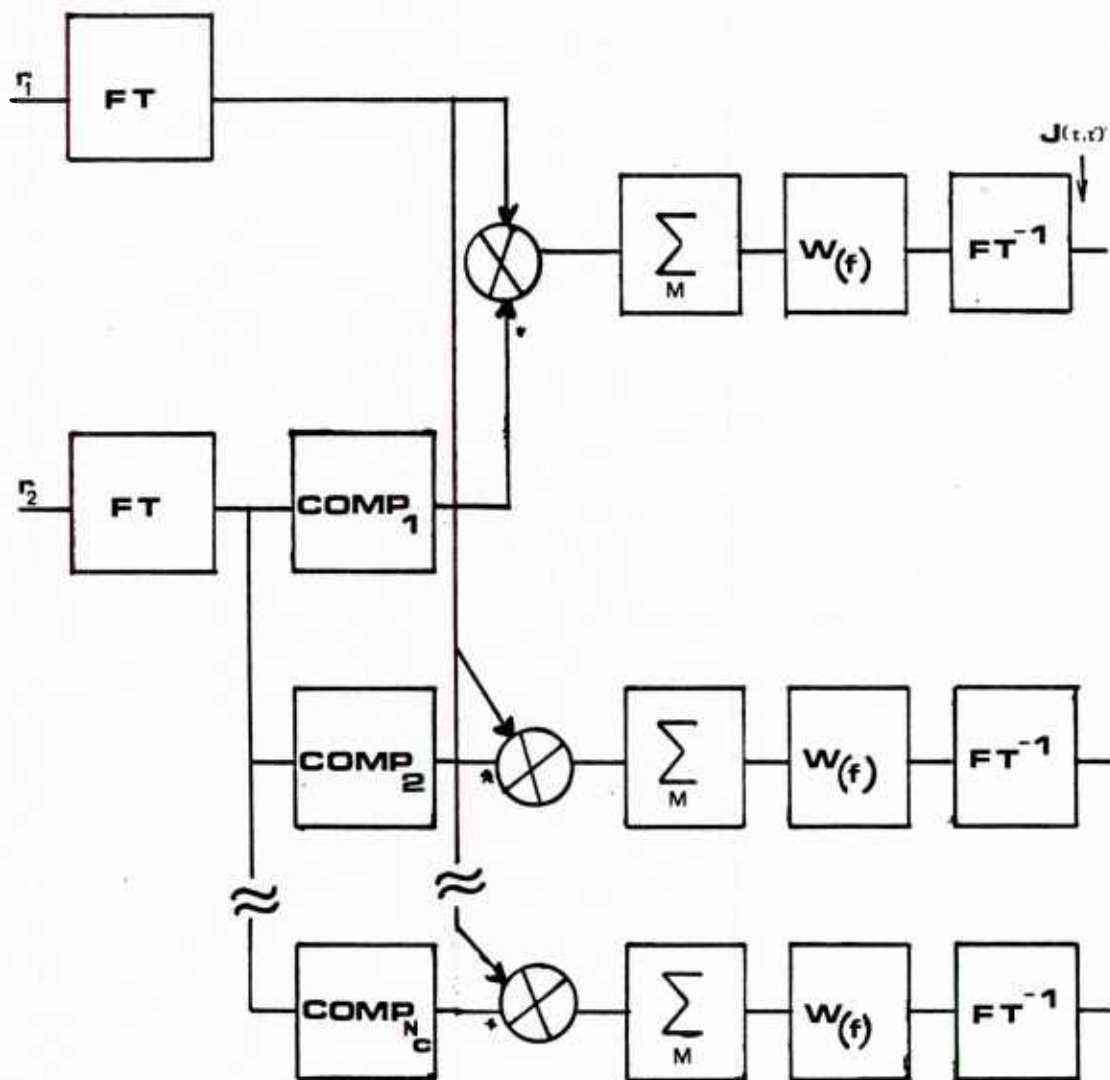


FIGURE 15
PHASE ROTATION COMPENSATION BLOCK DIAGRAM

equivalent no-motion GCC. This is done for a range of hypothesized τ' , again generating a two dimensional ambiguity surface from which the estimates for d' and d_0 are obtained. This process is illustrated in Figure 16.

The simulations reported in [38] verify that this method very nearly approximates the ML method of section 3.2, for a wide range of d' , and requires an order of magnitude fewer computations than the ML method.

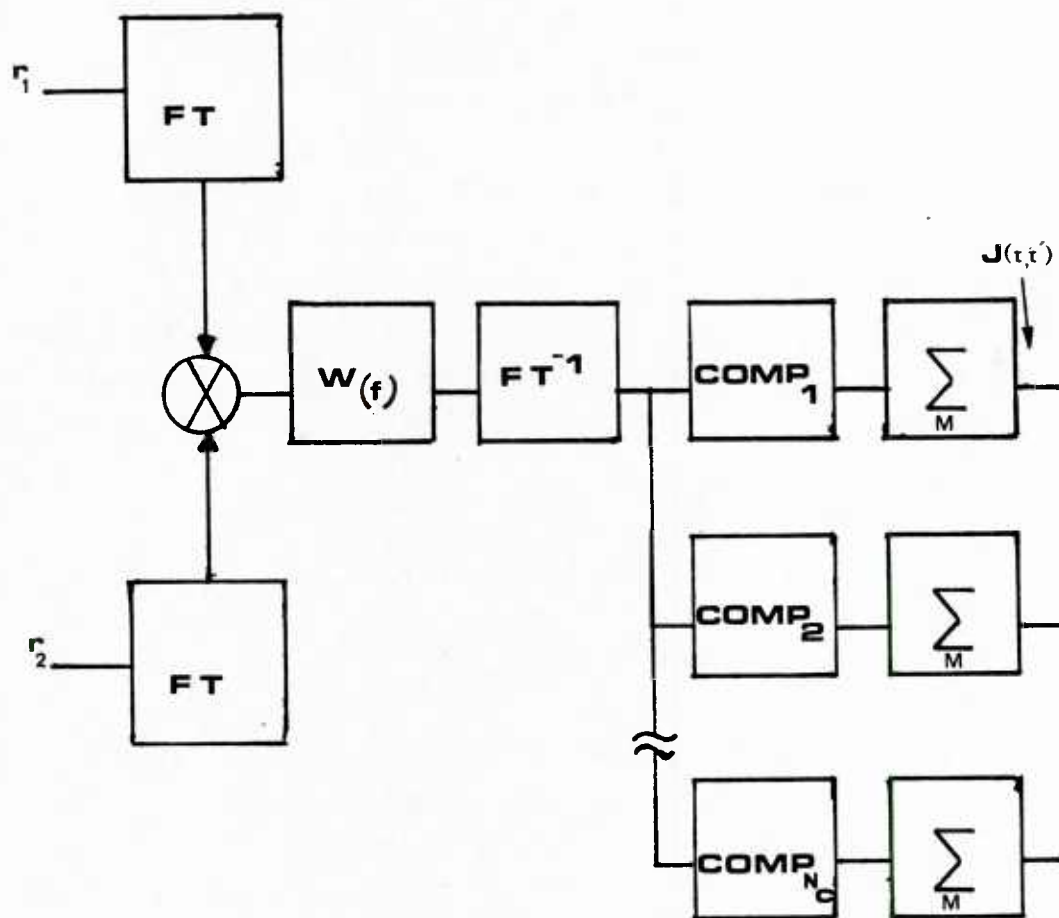


FIGURE 16
DESKEWING COMPENSATION BLOCK DIAGRAM

4.0 SIMULATION OF MOTION COMPENSATED TDE

A computer simulation of the motion compensated cross-correlator described in Section 3.3.1 was implemented on a Hewlett Packard HP9845B desktop computer, to experimentally observe the effects on performance when motion compensation is used or not used, when there is relative motion present. It was also done to verify some of the key theoretical analysis presented earlier, and to gain some insight into the problems associated with implementation. The simulation process, test run parameters, and test results and discussion are covered in the following subsections. A description of the simulation program is provided in Appendix A.

4.1 Simulation Description

4.1.1 Signal Generation

Simulated samples of the receiver signals $r_1(t)$ and $r_2(t)$ of (3.5) were generated as follows. Three independent Gaussian pseudo-random noise sequences, having zero-mean and unit variance, were generated from independent uniform, $[0,1]$, sequences by the "direct method" of [40, pp. 953]. One of these was used as the sample sequence $s(n)$ from $s(t)$. The other two, $n_1(n)$ and $n_2(n)$, were scaled according to the desired SNR, and represented samples from $n_1(t)$ and $n_2(t)$.

The $s(n)$, $n_1(n)$, and $n_2(n)$ sequences are next filtered with a Low-Pass 4-stage, 2-pole Butterworth IIR digital filter with $f_{\max} = 100$ Hz, the upper frequency of the pass band for an assumed sample rate of 2048 Hz.

The $s(n)$ sequence was processed by a time-varying filter function which introduced a phase shift that was linearly dependent on frequency, and was varied from time sample to time sample, according to the desired simulated delay rate, d' (41). The frequency dependent, linear phase shift in the frequency domain is equivalent to a delay in the time domain [19, pp. 66-67]. Varying this phase for each sample simulates a time-varying time delay, $d(n)$, that varies from sample to sample at the rate of d' sample intervals/sample interval. A relative attenuation, $\alpha=1$, is simulated. Finally $s(n)$ and $s(n+d(n))$ are added to $n_1(n)$ and $n_2(n)$ to get $r_1(n)$ and $r_2(n)$, the simulated samples from $r_1(t)$ and $r_2(t)$. Sequence lengths of 256 samples were used for each T_k interval.

4.1.2 Processing

The time-varying time-delay compensation technique of Section 3.3.1 was implemented as follows. Since the signal and noise generated have flat spectra and equal SNR across the band, an ML weight of $w^{ML}(f) = 1$ was used (i.e., the SCC weight). The frequency domain cross-correlation algorithm of [21, pp. 555-562] was used, with 512 point FFT's (including 256 augmenting zeroes), but prior to inverse transforming, the cross-spectra were phase rotated according to (3.13). Five hypothesized values for τ' were used: $-2/256$, $-1/256$, 0 , $1/256$, and $2/256$ seconds/second (or equivalently, sample intervals/sample interval). Each phase-rotated cross-spectrum was then summed and averaged with the corresponding ones from the previous intervals and

then inverse FFT'd after all M intervals had been processed. The five resulting cross-correlations thus formed a 5 by 512 point ambiguity surface in τ' , τ space. The global peak was determined and it's corresponding values for τ and τ' were used as the ML estimates of d_o and d' , respectively.

4.1.3 Simulation Parameters

The simulation was conducted using a total coherent integration time of $T = 2$ seconds, and an assumed sample rate of 2048 Hz . The total time, T , was sub-divided into sixteen $1/8$ second intervals (i.e. $M=16$) of 256 points each and processed as indicated above. SNR's ranging from -12dB to +6dB in 3dB steps were used, with 100 trials (2 seconds each) run at each SNR. Delay rates of $d' = \pm 1/256$ seconds/second and initial delays of $d_o = +16, -16$ and 0 samples were simulated. Statistics on the resulting delay, delay rate, and correlation peak amplitude were gathered for both compensated and uncompensated correlations.

4.1.4 Results

Figure 17 shows the compensated (by phase-rotation) short-time cross-correlations for each short segment in a single trial. The SNR was +6dB (this is the same trial illustrated in Figures 13 and 14).

Figure 18 is the ambiguity "surface" generated for the same trial shown in Figures 13, 14, and 17.

Table 2 lists the error performance, $\log_{10} \text{Stdv}[\hat{d}_o - d_o]$ for the delay estimates for compensated and uncompensated

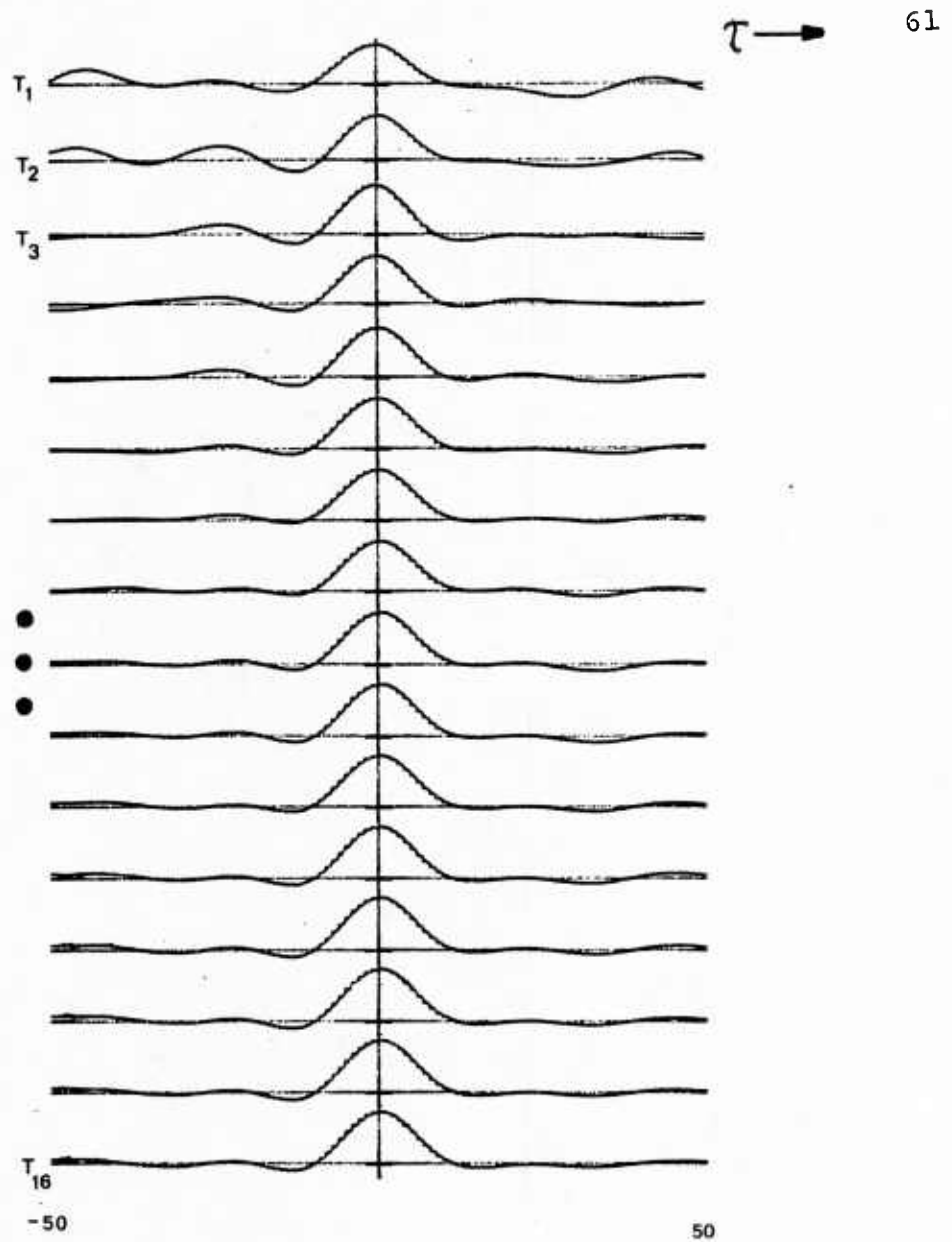


FIGURE 17
COMPENSATED SHORT-TIME CROSS-CORRELATIONS
(PHASE ROTATION METHOD)

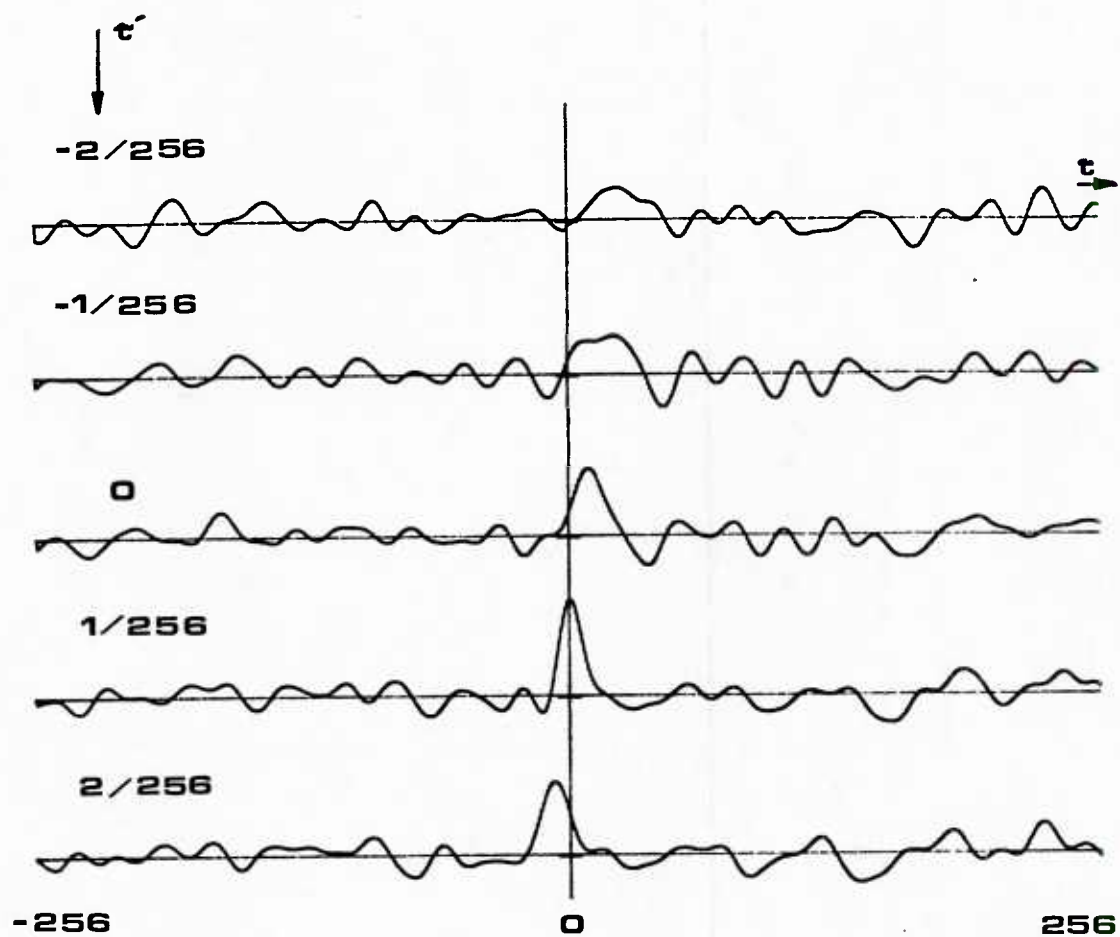


FIGURE 18
SAMPLE AMBIGUITY SURFACE

SNR(dB)	Log ₁₀ Stdv[$\hat{d}_o - d_o$]		Mean Peak Loss (dB)
	COMP	NO COMP	
6	0	-3.41	-1.63
3	-4.13	-3.36	-1.62
0	-3.68	-3.28	-1.60
-3	-3.46	-2.52	-1.58
-6	-1.59	-1.39	-2.25
-9	-1.22	-1.21	-2.72
-12	-1.16	-1.17	-4.16

TABLE 2
SIMULATED RUN STATISTICS

processing. The mean peak loss is defined as $10 \log_{10}$ of the ratio of the mean correlator peak value for the uncompensated processing to that of the compensated processing.

Figure 19 shows plots of the error performance for the simulation runs compared to those predicted by the CPE and CRLB. The x's are from a separate simulation reported in [32], for which there was no relative motion. The points marked with "dots" are from the simulation with motion reported here. Note that the vertical axis is in $\log_{10} \text{Std}[\hat{d}_0 - d_0]$. The confidence intervals, [20, pp. 113-115], are indicated. The upper plot shows the uncompensated performance, and the compensated results are shown in the lower plot.

4.1.5 Discussion

Figure 17 clearly shows the effectiveness in the compensation scheme for $d'=1/256$. The bottom correlation is the average of all 16 segments. The peak has been shifted back to the true value of $d_0=0$ as expected from (3.13).

Figure 18 shows the final corss-correlation from a single trial for each hypothesized τ' which, together, form the ambiguity surface. The center one corresponds to $\tau'=0$, or no compensation. Note the difference in its peak width and height compared to the correctly compensated correlation ($\tau'=1/256$), second from the bottom. As predicted earlier, the uncompensated correlation peak is both broader

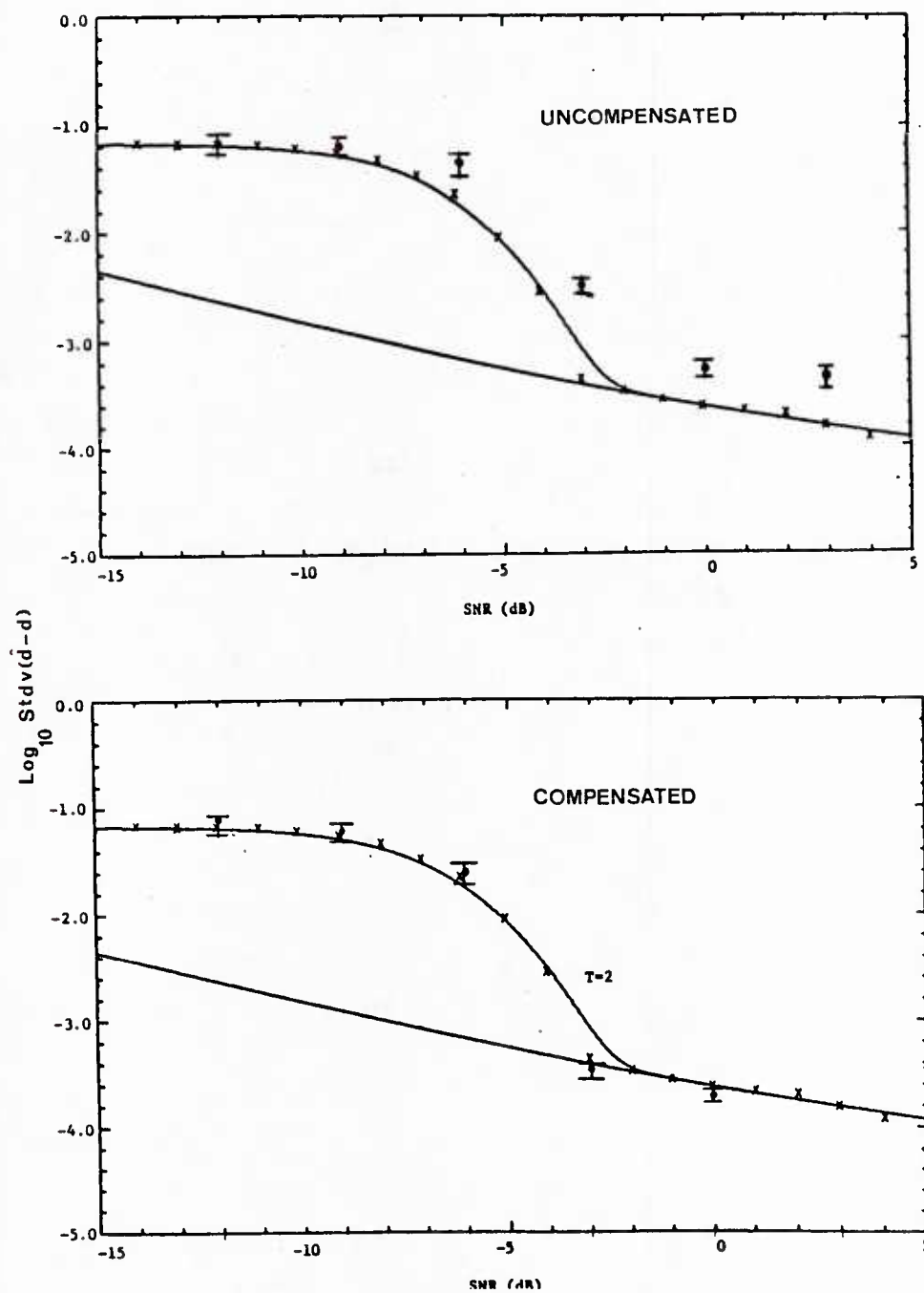


FIGURE 19
COMPENSATED VS. UNCOMPENSATED
PERFORMANCE, SIMULATION RESULTS

("smeared") and lower in amplitude, due to uncompensated averaging.

The performance plots of Figure 19 are consistent with the theory presented. The threshold SNR for the uncompensated estimates appears to occur at a higher SNR ($\cong + 1.5\text{dB}$ higher) than for the compensated correlations, which is consistent with the $\cong 1.6\text{dB}$ loss in peak value. Also, the error is greater at all SNRs above the threshold due to spreading and drop in amplitude of the uncompensated correlation peak which is expected to cause an increase in local error variation.

5.0 CONCLUSIONS AND RECOMMENDATIONS

The theory and analysis presented earlier had indicated that the GCC is a near optimum (when spectra must be estimated) estimator of time delay for fixed source and receivers. It was shown that the introduction of motion would require compensation for the effects of relative time-companding, or equivalently, time varying delay; otherwise a reduction in performance would be encountered. Several schemes for compensating for these effects were described and one using phase rotation of the estimated cross-spectra was implemented in the simulation program described in Appendix A. The results of running 100 trials for a range of SNR's are consistent with the theory and analysis presented earlier. In particular, compensated estimations performed near the optimum defined for the case with no-motion. The effect of no compensation was an overall increase in estimation error variance and an onset of anomalous errors at a higher SNR than for the compensated case.

The variety of the trials run for the simulation results presented here was very limited in scope due to the enormous computation times involved. Use of an array processor (such as reported in [32]), would greatly expand the number possible run parameters which could be simulated.

It is recommended that more simulations be run using a wider range of delay rates. Also, simulation results are needed which use a larger number of hypothesized delay-rate compensations, to determine the effects that more points on the ambiguity surface might have on the number of

occurrences of anomalous peaks. Finer SNR steps would help to better define the shape of the performance curves, allowing a more accurate empirical comparison of error performances.

LIST OF REFERENCES

1. W. C. Knight, R. G. Pridham, and S. M. Kay, "Digital Signal Processing for Sonar," Proc. IEEE, vol. 69, no. 11, pp. 1451-1506, Nov 1981.
2. A. B. Baggeroer, "Sonar Signal Processing." in Applications of Digital Signal Processing, ed. A.V. Oppenheim. Englewood Cliffs, N.J.; Prentice Hall, 1978, pp. 331, 437.
3. R. J. Urick, Principles of Underwater Sound. New York: McGraw-Hill, 1983.
4. C. W. Horton, Sr., Signal Processing of Underwater Acoustic Waves, U. S. Government Printing Office, 1969 (lib. of Congress Cat. No. 74-603409).
5. G. C. Carter, Ed., Special Issue on Time Delay Estimation, IEEE Trans. Acoust., Speech, Signal Processing, Vol. ASSP-29, No. 3, June 1981.
6. Shearwater Inc., Final Report: An Overview of Inter-Array Processing For a Two Array System, Prepared for Naval Underwater Systems Center, New London Laboratory, New London, CT, Contract No. N00140-79-D-6671, October 1981.
7. C. H. Knapp and G. C. Carter, "The Generalized Correlation Method for Estimation of Time Delay," IEEE Trans. Acoust., Speech, Signal Processing, Vol. ASSP-24, pp. 320-327, Aug. 1976.
8. P. R. Roth, "Effective Measurements Using Digital Signal Analysis," IEEE Spectrum, vol. 8, pp. 62-70, Apr 1971.
9. G. C. Carter, A. H. Nuttall, and P. G. Cable, "The Smoothed Coherence Transform," Proc. IEEE, vol. 61, pp. 1497-1498, Oct 1973.
10. ———, "The Smoothed Coherence Transform (SCOT)," Naval Underwater Systems Center, New London, CT, Tech. Memo. TL-159-72, 8 Aug 1972.
11. C. Eckart, "Optimal Rectifier Systems for Detection of Steady Signals," Scripps Inst. Oceanography, Marine Physical Lab., Rep. SIO 12692, SIO Ref. 52-11, 1952.

12. E. J. Hannan and P. J. Thomson, "Estimating Group Delay," Biometrika, vol. 60, no. 2, pp. 241-253, 1973.
13. K. Scarbrough, Analysis of Time Delay Estimator Performance, Ph.D. Dissertation, Kansas State University, 1984.
14. K. Scarbrough, N. Ahmed, and G. C. Carter, "Comparison of Two Methods for Time Delay Estimation of Sinusoids," Proc. IEEE (Corr.), Vol. 70, No. 1, pp. 90-92, Jan 1982; see also K. Scarbrough, N. Ahmed, D. H. Youn, and G. C. Carter, "On the SCOT and Roth Algorithms for Time Delay Estimation," in Proc. IEEE Int. Conf. Acoust., Speech, Signal Processing, pp. 371-374, 1982.
15. K. Scarbrough, N. Ahmed, and G. C. Carter, "On the Simulation of a Class of Time Delay Estimation Algorithms," IEEE Trans. Acoust., Speech, Signal Processing (Corr.), Vol. ASSP-29, No. 3, pp. 534-540, June 1981.
16. J. C. Hassab and R. E. Boucher, "A Quantitative Study of Optimum and Suboptimum Filters in the Generalized Correlator," in Proc. 1979 IEEE Int. Conf. Acoust., Speech, Signal Processing, pp. 124-127, 1979.
17. A. Papoulis, Probability, Random Variables, and Stochastic Processes. New York: McGraw-Hill, 1965.
18. G. M. Jenkins and D. G. Watts, Spectral Analysis and its Applications. San Francisco, CA: Holden Day, 1968.
19. J. S. Bendat and A. G. Piersol, Engineering Applications of Correlation and Spectral Analysis. New York: Wiley, 1980.
20. J. S. Bendat and A. G. Piersol, Random Data: Analysis and Measurement Procedures. New York: Wiley-Interscience, 1971.
21. A. V. Oppenheim and R. W. Schaffer, Digital Signal Processing. Englewood Cliffs, NJ: Prentice-Hall, 1975.
22. IEEE ASSP Digital Signal Processing Committee Ed., Programs for Digital Signal Processing. New York: IEEE Press, 1979.

23. G. C. Carter and A. H. Nuttall, "On the Weighted Overlapped Segment-Averaging Method for Power Spectral Estimation," Proc. IEEE, Vol. 68, No. 10, pp. 1351-1354, Oct. 1980.
24. V. H. MacDonald and P.M. Schulteiss, "Optimum Passive Bearing Estimation," J. Acoust. Soc. Amer., Vol. 46, pp. 37-43, 1969.
25. H. L. Van Trees, Detection, Estimation, and Modulation Theory - Part I. New York: Wiley, 1968.
26. A. H. Quazi, "An Overview of the Time Delay Estimate in Active and Passive Systems for Target Localization," IEEE Trans. Acoust., Speech, Signal Processing, Vol. ASSP-29, No. 3, pp. 534-540, June 1981.
27. J. M. Wozencraft and I. M. Jacobs, Principles of Communication Engineering. New York: Wiley, 1965.
28. A. Weiss and E. Weinstein, "Composite Bound on the Attainable Mean-Squared Error in Passive Time Delay Estimation from Ambiguity Prone Signals," IEEE Trans. Info. Theory (Corr.), Vol. IT-28, No. 3, pp. 977-979, Nov 1982.
29. J. P. Ianniello, "Time Delay Estimation via Cross-Correlation in the Presence of Large Estimation Errors," IEEE Trans. Acoust., Speech, Signal Processing, Vol. ASSP-30, No. 6, pp. 998-1003, Dec 1982.
30. E. Weinstein, "Performance Analysis of Time Delay Estimators," Woods Hole Oceanographic Institute, Woods Hole, Mass., WHOI Technical Report, 1983.
31. J. P. Ianniello, E. Weinstein, and A. Weiss, "Comparison of the Ziv-Zakai Lower Bound on Time Delay Estimation with Correlator Performance," in Proc. 1983 Int. Conf. Acoust., Speech, Signal Processing, pp. 875-878, 1983.
32. K. Scarbrough, R. Tremblay, and G. C. Carter, "Performance Predictions for Coherent and Incoherent Processing Techniques of Time Delay Estimation," IEEE Trans. Acoust., Speech, Signal Processing, Vol. ASSP-31, No. 5, pp. 1191-1196, Oct 1983.

33. A. H. Nuttall, "Threshold Signal-To-Noise Ratio For Time Delay Estimation Via Cross-Correlation," Naval Underwater Systems Center, New London, CT, NUSC Tech. Memo 831065, April 1983.
34. W. B. Adams, J. P. Kuhn, and W. P. Whyland, "Correlator Compensation Requirements for Passive Time-Delay Estimation With Moving Source or Receivers," IEEE Trans. Acoust., Speech, Signal Processing, Vol. ASSP 28, No. 2, 158-168, April 1980.
35. C. H. Knapp and G. C. Carter, "Estimation of Time Delay in the Presence of Source or Receiver Motion," J. Acoust. Soc. Am., Vol. 61, No. 6, pp. 1545-1549, June 1977.
36. J. P. Kuhn, S. E. Robison, and D. W. Winfield, "Time Delay Estimation Techniques for Moving Sources," in Proc. 24th Midwest Symp. Circuits and Syst., pp. 69-75, June 1981.
37. G. W. Johnson, E. E. Ohlms, and M. L. Hampton, "Broadband Correlation Processing," Proc. 1982 Conf. Acoust. Speech Signal Proc., pp. 583-586, 1983.
38. J. W. Betz, "Comparison of the Deskewed Short-Time Correlator and the Maximum Likelihood Correlator," IEEE Trans. Acoust., Speech, Signal Processing, Vol. ASSP-32, No. 2, pp. 285-294, April 1984.
39. J. W. Betz and K. R. Harberl, "Implementation of the Time-Companding Correlator Using Numerical Interpolation," RCA Rept. BNAS-83-TR-014, May 1983.
40. M. Abramowitz and I. A. Stegun, Ed., Handbook of Mathematical Functions, Tenth Printing. U. S. Government Printing Office, Washington, D.C., 1972.
41. D. H. Youn, N. Ahmed, and G. C. Carter, "A method for generating a class of time-delayed signals," in Proc. 1981 IEEE Int. Conf. Acoust., Speech, Signal Processing, pp. 1257-1260, 1981.

APPENDIX A

Figure A.1 is a program structure chart indicating the subroutines of the simulation program and their relationship to each other. Figure A.2 is a functional flow chart indicating the top-level flow of the simulation program process.

For listings or program copies contact:

R. J. Tremblay, Code 3314
Naval Underwater Systems Center
New London, Connecticut 06320

or

Professor D. W. Lytle
EE Building, FT-10
University of Washington
Seattle, Washington 98195

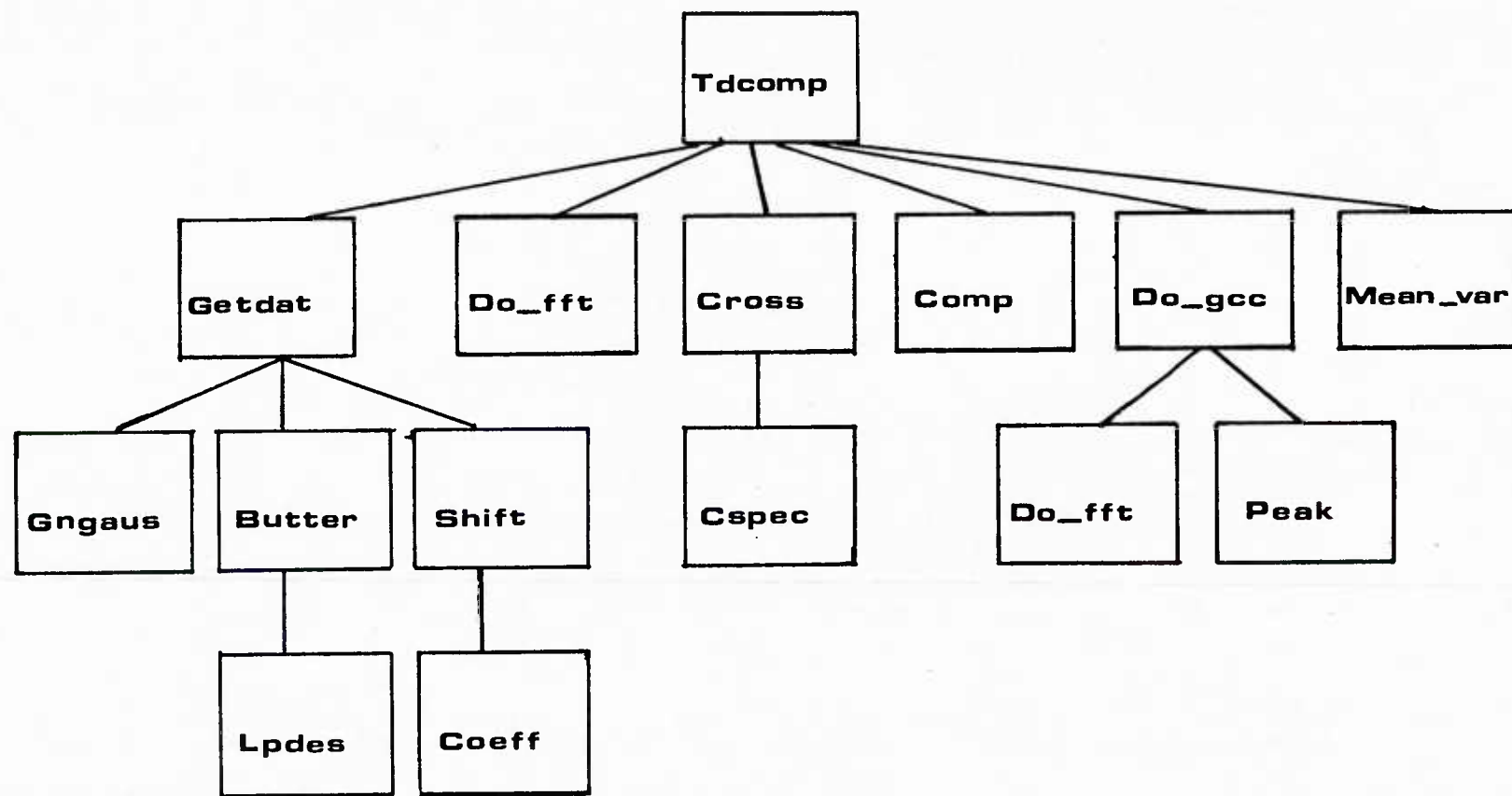


FIGURE A.1
PROGRAM STRUCTURE CHART

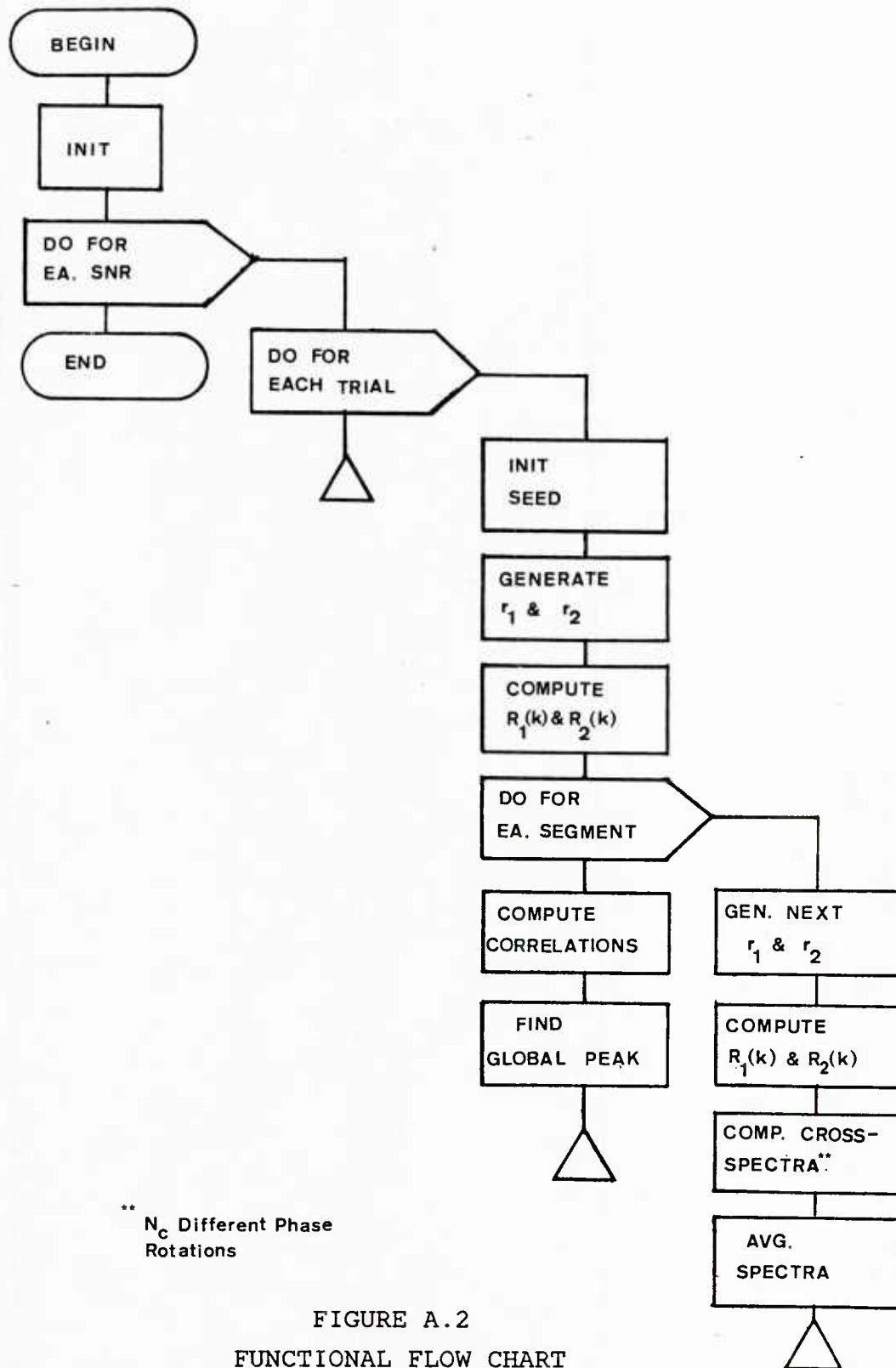


FIGURE A.2
FUNCTIONAL FLOW CHART

INITIAL DISTRIBUTION LIST

Addressee	No. of Copies
NRL	5
NAVSEASYSOM, SEA-63D (2), -63R (2), PMS-409 (3), -411 (3)	10
NAVAIRDEVCE	5
NOSC, Code 8302	5
NCSC, Code 724	5
NAVSWC	5
DWTNSRDC ANNA	2
DWTNSRDC BETH, Code U31	2
NAVPGSCOL	1
DARPA	1
NAVSURWEACTR	1
DTIC	12

U213200

